scientific reports



OPEN

Antiproliferation, 3D-multicellular spheroid and VEGFR-2 inhibitory properties of spiroindolin-2-ones with phosphonate function

Sara M. Hassan¹, Alyaa Farid¹, Mohamed S. Bekheit^{2⊠}, Siva S. Panda^{3,4}, Benson M. Kariuki⁵, Anwar Abdelnaser⁶, Soad Nasr⁶, Walid Fayad⁷, May A. El-Manawaty⁷, Ahmed A. F. Soliman⁷ & Adel S. Girgis^{2™}

Spiroindolin-2-ones with phosphonate function 17a-t (20 analogs, 96-72% yield) were generated by microwave synthetic methodology using azomethine cycloaddition of the appropriate 3,5-bis(ylidene)-4-piperidone-1-phosphonate 14a-q. Single crystal X-ray analysis of 17d confirmed the structure. Promising 2D-monolayer antiproliferation properties (MTT assay) were observed for some of the synthesized agents with no harm to normal (RPE1) cell line. Compound 17h (R = 4-ClC₆H₄, R' = H; $IC_{so} = 3.08 \mu M$; 6.6- and 3.1-fold the standard drugs, 5-fluorouracil and sunitinib, respectively) is the most distinguished agent against colon/HCT116 cell line. Compound 17f (R = 4-FC, H,, R' = Cl; $IC_{so} = 5.252 \mu M$; 3.2-fold the activity of sunitinib, the clinically approved standard drug) also has significant activity against pancreatic/PaCa2 cell line. 3D-multicellular spheroid (HCT116) testing was also performed. Notable VEGFR-2 inhibitory properties were evident for some of the synthesized analogs. Considerable activity against COX-1/-2 and TNF- α , relative to the established NSAIDs ibuprofen and indomethacin, was also detected. CAM testing evidenced the anti-VEGFR-2 observations and anti-angiogenic properties. Internal and external validated QSAR models explored the functions necessary for the antiproliferation potency. In conclusion, the designed spiroindolin-2ones conjugated with phosphonate function can be useful for optimizing novel anti-cancer therapeutic agent(s) with anti-angiogenic (anti-VEGFR-2) mode of action after considering more needed advanced pharmacological studies.

Keywords Spiroindolin-2-one, Cancer, Antiproliferation, 3D-spheroid, VEGFR-2

Angiogenesis is a key physiological process necessary for delivering nutrients, metabolites and oxygen to endothelial cells besides the disposal of waste products, including carbon dioxide. It involves the development of new capillaries and eventually the formation of the blood vascular network from pre-existing vasculature. The process is important in a range of normal and therapeutic processes, including embryogenesis, wound healing and muscle repair, ischemic and peripheral arterial diseases and the menstrual cycle. Some pathological conditions, such as arthritis, atherosclerosis, and some solid cancerogenesis development and metastasis, are characterized by uncontrolled angiogenesis¹⁻⁴. An approach to combating various types of cancer that has received a lot of attention in medicinal chemistry targets the design and synthesis of promising angiogenesis inhibition agents. Some anti-angiogenic small molecules have been investigated against various cancer types and awarded Food and Drug Administration (FDA) approval⁵⁻²⁰ (Fig. 1).

Multiple angiogenic proteins have been identified, one family of which is the vascular endothelial growth factors (VEGF), which are tyrosine kinases hyperactivated in cancer cells. The two main categories of tyrosine

¹Biotechnology Department, Faculty of Science, Cairo University, Giza, Egypt. ²Department of Pesticide Chemistry, National Research Centre, Dokki, Giza 12622, Egypt. ³Department of Chemistry and Biochemistry, Augusta University, Augusta, GA 30912, USA. ⁴Department of Biochemistry and Molecular Biology, Augusta University, Augusta, GA 30912, USA. ⁵School of Chemistry, Cardiff University, Main Building, Park Place, Cardiff CF10 3AT, UK. ⁶Institute of Global Health and Human Ecology, School of Sciences and Engineering, The American University in Cairo (AUC), Cairo 11835, Egypt. ⁷Drug Bioassay-Cell Culture Laboratory, Pharmacognosy Department, National Research Centre, Dokki, Giza 12622, Egypt. [⊠]email: M_bekheit@yahoo.com; mb.hassan@nrc.sci.eg; girgisas10@yahoo.com; as.girgis@nrc.sci.eg

Sorafenib (Nexavar) is a kinase inhibitor approved for advanced renal cell (2005), hepatocellular (2007), and thyroid (2013) cancers^{5,6}.

Lenvatinib (Lenvima) is VEGFR-1, -2, -3; FGFR-1, -2, -3, -4; and PDGFR α inhibitor awarded approval for differentiated thyroid (2015), advanced renal cell (2016), and hepatocellular (2018) cancers^{9,10}.

Vandetanib (Caprelsa) is a kinase inhibitor for thyroid cancer (2011)^{13,14}.

Axitinib (Inlyta) is a VEGFR-1, -2, and -3 inhibitor for advanced renal cell (2019) cancer^{17,18}.

Regorafenib (Stivarga) is a multi-kinase inhibitor approved for advanced colorectal (2012), advanced gastrointestinal stromal (2013), and hepatocellular (2017) cancers^{7,8}.

Cabozantinib (Cabometyx) is a tyrosine kinase inhibitor approved for advanced renal cell (2017), hepatocellular (2019), and thyroid (2021) cancers^{11,12}.

Pazopanib (Votrient) is a kinase inhibitor for advanced renal cell (2009), and advanced soft tissue sarcoma (2012)^{15,16}.

Sunitinib (Sutent) is a multi-targeted tyrosine kinase inhibitor (VEGFR-1,-2, -3; PDGFR- α , - β ; and c-kit) against gastrointestinal stromal, advanced renal cell (2006), pancreatic (2011), and recurrent renal cell (2017) cancers ^{19,20}.

kinases are receptors and non-receptors. The receptor type is trans-membrane (extracellular or intracellular) whereas the non-receptor type is only intracellular. VEGF sub-types include VEGF-A, -B, -C, -D, and -E, but only the first four subtypes are naturally found in the human genome. They are generally categorized according to their binding into receptors VEGFR-1, -2, and -3^{21-23} . Anti-VEGFR-2 agents have been reported to be promising hits and/or leads against many solid cancer types (lung, breast, colon, renal, skin, etc.)^{21,24-26}.

Indolin-2-one is a heterocyclic motif that has progressively gained interest in the last decades due to the biological properties associated with the developed new analogs²⁷. Sunitinib (Sutent) 8 is an analog that has famously gained FDA approval for clinical use against gastrointestinal stromal, advanced renal cell (2006), pancreatic (2011), and recurrent renal cell (2017) cancers with a multi-targeted tyrosine kinase (VEGFR-1,-2, -3; PDGFR-α, -β; and c-kit) inhibitory effect^{19,20,28} (Fig. 1).

The study adopts synthesis of spiroindolin-2-one analogs collaborating with phosphonate group. The phosphonate group is isosteric to the phosphate group. Some phosphonate compounds are well known drugs, including adefovir 9²⁹, cidofovir 10³⁰ (antiviral), and zoledronic acid 11³¹ (anti-osteoporotic), or pro-drugs such as adefovir dipivoxil 12 (a pro-drug of adefovir)³² and tenofovir disoproxil 13 (a pro-drug of tenofovir phosphonate³³, which is used to treat hepatitis B). Phosphate esters are highly successful in enhancing the delivery of drug and/or drug candidates that are poorly soluble in water following oral administration^{34,35}. Thus, judicious modification of the target agent can elevate its potency³⁶ (Fig. 2).

The current study is directed towards synthesizing spiro-indolin-2-one-containing compounds and investigating their antiproliferation properties against a variety of human cancer cell lines with determination of their mode of action as anti-angiogenic agents against VEGFR-2. Interest in this subject is attributed to the antitumor properties associated with the structure of the targeted scaffold and continuation of our efforts in this drug discovery program directed towards exploring antiproliferation properties of spiroindolin-2-one containing compounds³⁷⁻⁴¹. The reason for addition of the phosphonate group into the targeted analogs is due to the associated hydrophobic properties that may positively impact the overall pharmacokinetic properties of the designed agents. The pro-drug design approach is a viable option to achieve enhanced bioavailability of a drug candidate characterized by low hydrophilicity and poor cell membrane permeability. Functionalizing the drug candidate with a moiety like carboxylic, carbonyl, carboxamide, or phosphate/phosphonate groups is one of the most effective pro-drug design approaches for a wide range of drug molecules⁴². Incorporation of an ionizable group, such as phosphate, amino acid and sugar moieties, in the promising agents/drug candidates results in enhancement in aqueous solubility, which helps to achieve the desired bioavailability of the pharmaceutically active potential molecule(s)³⁴. This justifies the collaboration of the phosphonate group with the targeted spiroheterocyclic scaffold in this work. Some of the targeted analogs have been investigated by our group, revealing promising antiviral properties with potential M^{pro}-SARS-CoV-2 inhibitory effect⁴³. Clinical trials supported the ability of treating colon cancer patient with viral infection by either antiviral drug alone or in combination with anticancer drug(s)44 motivated our previous work for investigating their antiviral properties. However, the current work moved towards antiproliferation properties investigation of the synthesized spiroindolin-2-one analogs conjugated with phosphonate group against a variety of cancer types and focusing on studying their

Fig. 2. Drugs/pro-drugs with phosphonate group.

mode of action against VEGFR-2 motivated by the reported anti-cancer properties of the adopted chemical scaffold^{37–41}.

Results and discussion Design of the targeted agents

The current study is directed towards development of spiroindolin-2-one analogs conjugated with a phosphonate group of potential antiproliferation properties against a variety of cancer cell lines. The main heterocyclic core (spiroindolin-2-one) is responsible for the antiproliferation properties of the targeted agents^{37–41}. The conjugated phosphonate group can assist in the delivery of the drug candidates^{34–36}. Meanwhile, variation of R and R' is adopted for optimizing a high effective/potent agent(s) (Fig. 3).

Chemical synthesis

Microwave-assisted dipolar cycloaddition towards the targeted spiroindolin-2-ones bearing phosphonate group 17a-t were generated in high yield (96-72%) through reaction of non-stabilized azomethine ylides (produced during the interaction "in-situ" from isatins 15a-d and sarcosine 16) with the activated olefinic bond of piperidines 14a-g⁴³ (Fig. 4). ¹H-NMR showed the methylene groups of piperidone (H_2 C-2" and H_2 C-6") and pyrrolidine (H_2 C-5) heterocycles as diastereotopic protons. The multiple signals of the methyl and methylene carbons of phosphonate groups are due to the effect of phosphorus atom. Regioselectivity of the reaction seems a general characteristic function associated with the azomethine cycloaddition under the applied experimental conditions⁴³. Single crystal X-ray characterization of 17d evidenced the chemical structure.

Crystal structure of 17d

The crystal structure is triclinic, P-1 (Supplementary Table S1), and the asymmetric unit contains one molecule of 17d and half a molecule of methanol (solvent of crystallization) which is disordered on an inversion symmetry center. At the center of the molecule of 17d (Fig. 5) is a 2,7-diazaspiro[4.5]decan-10-one ring system comprising a pyrrolidine ring (PYR: C8 – C12, N2) and a piperidin-4-one (PIP: C10, C20-C23, N3, O2) group. The pyrrolidine ring is in chair conformation with the methylene group as the flap and the piperidin-4-one ring is in an unsymmetrical chair conformation. The 1,3-dihydro-2*H*-indol-2-one group (DHI: C2 – C9, N1, O1) is planar and is connected to the pyrrolidine ring through the shared atom C8. The linked PYR, PIP and DHI groups form a core with limited flexibility whereas phenyl (C14-C19), methylbenzene (C28-C34) and diethylphosphonate (C24-C27, O3 O5, P1) groups introduce more conformational flexibility to the molecule. In the crystal, pairs of molecules of 17d are linked by two N-H...O across an inversion center. The N-H group is the donor, and the acceptor is the diethyl phosphonate oxygen, with a N1-H1...O3 angle of 164.7° and N1...O3 distance of 2.828(2) Å. An O-H...O hydrogen bond is also observed between the methanol molecule and the piperidin-4-one oxygen, with a O6-H6A...O2 angle of 171.0° and O6...O2 distance of 2.926(7) Å.

Biological studies

2D-Monolayer antiproliferation properties

The MTT [3-(4,5-dimethylthiazol-2-yl)-2,5-diphenyl-tetrazolium bromide] to purple formazan standard technique was adopted for studying the 2D-monolayer antiproliferation properties of the synthesized analogs 17a-t against a set of cancer cell lines (HCT116/colon, PaCa2/pancreatic, MCF7/breast, and A549/lung) in addition to normal (RPE1 "retinal pigment epithelial") cell for determining the safety index/behavior^{30,45}. The properties were compared with clinically approved anticancer drugs including sunitinib (gastrointestinal, renal, and pancreatic cancer)^{19,20}, 5-fluorouracil (colon, rectum, breast and skin)^{46,47}, and doxorubicin (broad spectrum anti-cancer drug against many cancer types, including breast, lung, gastric, and ovarian)⁴⁸. The results are presented in Table 1 and Supplementary Figs. S25-S29.

<u>HCT116</u> Colon cancer is one of the most prevalent malignant tumors of the digestive system worldwide and is ranked second of all cancers based on mortality rate. Environmental, dietary, and lifestyle factors are connected

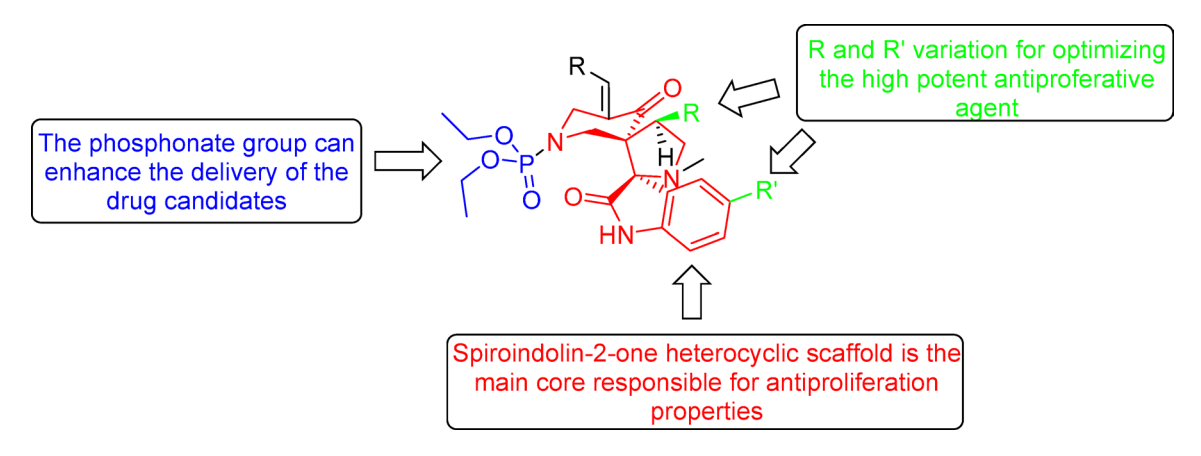


Fig. 3. Design of the targeted agents.

Fig. 4. Synthetic route towards the targeted agents 17a-t.

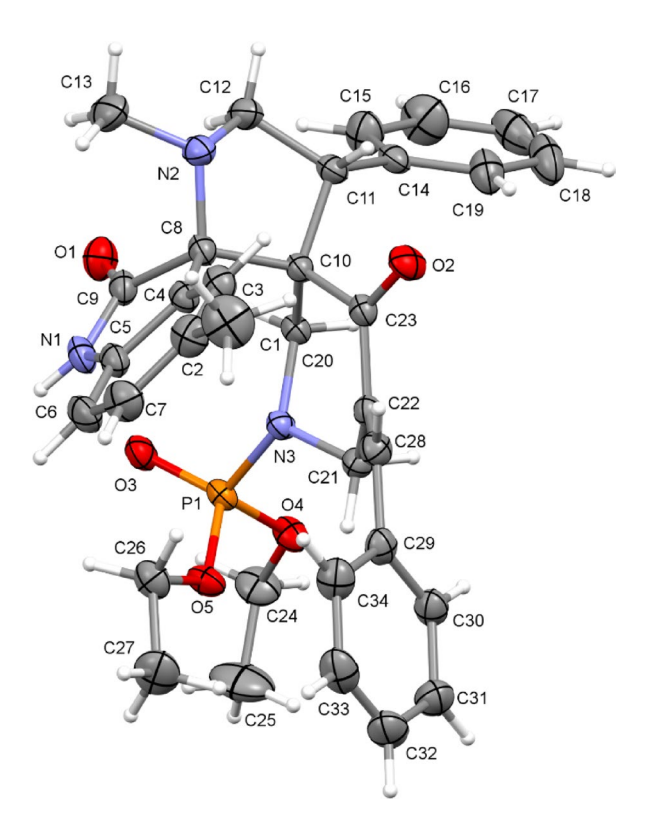
to its incidence. Although many chemotherapeutics have been developed and some have been awarded clinical approval, the limited efficacy especially towards the advanced, recurrent, and metastatic conditions as well as the associated side effects drives the need for newer agents^{49,50}.

All the agents synthesized in this investigation exhibited higher anti-HCT116 efficacies than the clinically approved drug 5-fluorouracil (IC $_{50}$ = 20.43 μM). Compound 17h (R=4-ClC $_6H_4$, R'=H) is the most promising of the agents with potency IC $_{50}$ = 3.08 μM (6.6- and 3.1-folds of the standard drugs 5-fluorouracil and sunitinib, respectively). Compounds 17f (R=4-FC $_6H_4$, R'=Cl), 17j (R=4-ClC $_6H_4$, R'=Cl), 17k (R=4-ClC $_6H_4$, R'=Me) 17m (R=4-H $_3$ CC $_6H_4$, R'=H) and 17o (R=4-H $_3$ CC $_6H_4$, R'=Cl) also had high efficacies (IC $_{50}$ =3.281-3.756 μM).

Based on the observed anti-HCT116 properties, some SARs (structure–activity relationships) can be deduced. The 4-chlorophenyl-containing analogs show enhanced anti-HCT116 properties relative to the other halogen-containing compounds as noted in 17h/17e/17l (IC $_{50}$ =3.080/6.989/4.162 μ M, respectively), 17j/17f (IC $_{50}$ =3.487/3.716 μ M, respectively), and 17k/17g (IC $_{50}$ =3.281/5.006 μ M, respectively). Similarly, the 4-methycontaining analog has better anti-HCT116 properties than the 4-methoxy-containing compound as shown by 17m/17p (IC $_{50}$ =3.438/5.512 μ M, respectively). The 5-chloroindolyl-containing compounds have greater anti-HCT116 properties than the 5-fluoroindolyl analogs as noted in pairs 17c/17b (IC $_{50}$ =6.317/7.409 μ M, respectively), 17j/17i (IC $_{50}$ =3.487/4.142 μ M, respectively), 17o/17n (IC $_{50}$ =3.756/5.095 μ M, respectively), and 17s/17r (IC $_{50}$ =5.416/7.670 μ M, respectively) (Fig. 6).

<u>PaCa2</u> Pancreatic cancer is one of the most aggressive forms of the disease (often referred to as the king of cancers) with a low five-year survival rate (\approx 10%) and high recurrence rates⁵¹. Patients diagnosed with pancreatic cancer are usually 40–85 years old⁵². Difficulties in early diagnosis, due to non-specific symptoms, in addition to the ability for migration and metastasis account for the survival rates⁵³.

All agents 17a-t show efficacy against PaCa2 cell line with higher potencies or close to that of sunitinib (clinically approved drug against pancreatic cancer, IC $_{50}$ =16.91 μ M). Compound 17f (R=4-FC $_{6}$ H $_{4}$, R'=Cl) is the most promising anti-PaCa2 agent observed (IC $_{50}$ =5.252 μ M, i.e. 3.2-fold that of the standard drug). Notable efficacy is also observed for compound 17m (R=4-H $_{3}$ CC $_{6}$ H $_{4}$, R'=H; IC $_{50}$ =5.605 μ M). Additionally, compounds



 $\textbf{Fig. 5}. \ \ \text{An Ortep representation of the molecule from the crystal structure of compound 17d.}$

| | IC ₅₀ , μM±SEM (SI ^a) | | | | | | |
|-------------------------------|--|------------------------|------------------------|-------------------------|--------------------|--|--|
| Compd | HCT116 | PaCa2 | MCF7 | A549 | RPE1 | | |
| 17a | 7.971 ± 0.338 (2.1) | 12.920 ± 0.559 (1.3) | 5.857 ± 0.259 (2.9) | 14.450 ± 0.259 (1.2) | 16.790 ± 0.516 | | |
| 17b | 7.409 ± 0.228 (3.1) | 12.230 ± 0.297 (1.9) | 5.826 ± 0.213 (4.0) | 10.990 ± 0.135 (2.1) | 23.100 ± 0.884 | | |
| 17c | 6.317 ± 0.132 (2.2) | 9.148 ± 0.154 (1.5) | 5.269 ± 0.172 (2.6) | 12.540 ± 0.205 (1.1) | 13.750 ± 0.423 | | |
| 17d | 9.278 ± 0.084 (1.9) | 15.570 ± 0.329 (1.2) | 5.782 ± 0.130 (3.1) | 14.590 ± 0.270 (1.2) | 17.900 ± 0.945 | | |
| 17e | 6.989 ± 0.101 (2.4) | 9.479 ± 0.278 (1.8) | 5.640 ± 0.273 (2.9) | 7.727 ± 0.155 (2.1) | 16.600 ± 0.907 | | |
| 17f | 3.716±0.099 (10.7) | 5.252 ± 0.224 (7.6) | 5.289 ± 0.175 (7.5) | >50.000 ± 2.111 (< 0.8) | 39.890 ± 1.162 | | |
| 17g | 5.006 ± 0.364 (3.8) | 6.092 ± 0.132 (3.1) | 5.426 ± 0.152 (3.5) | 8.149 ± 0.277 (2.3) | 19.040 ± 0.647 | | |
| 17h | 3.080 ± 0.165 (2.6) | 6.354 ± 0.170 (1.3) | 4.067 ± 0.054 (2.0) | 4.149 ± 0.288 (2.0) | 8.147 ± 0.675 | | |
| 17i | 4.142 ± 0.042 (> 12.1) | 13.450 ± 0.898 (> 3.7) | 4.808 ± 0.148 (> 10.4) | >50.000 ± 1.431 (-) | >50.000 ± 1.173 | | |
| 17j | 3.487 ± 0.033 (> 14.3) | 6.930 ± 0.337 (> 7.2) | 3.874 ± 0.102 (> 12.9) | 6.059 ± 0.157 (> 8.3) | > 50.000 ± 1.491 | | |
| 17k | 3.281 ± 0.022 (2.5) | 6.659 ± 0.095 (1.2) | 4.978 ± 0.095 (1.6) | 6.467 ± 0.385 (1.3) | 8.150 ± 0.507 | | |
| 171 | 4.162 ± 0.129 (1.9) | 6.151 ± 0.413 (1.3) | 4.852 ± 0.082 (1.6) | 7.281 ± 0.316 (1.1) | 7.848 ± 0.284 | | |
| 17m | 3.438 ± 0.083 (2.8) | 5.605 ± 0.063 (1.7) | 4.210 ± 0.085 (2.3) | 8.182 ± 0.435 (1.2) | 9.569 ± 0.537 | | |
| 17n | 5.095 ± 0.191 (> 9.8) | 15.340 ± 0.911 (> 3.3) | 4.368 ± 0.156 (> 11.5) | >50.000 ± 1.752 (-) | > 50.000 ± 1.739 | | |
| 17o | 3.756 ± 0.064 (> 13.3) | 6.273 ± 0.148 (> 8.0) | 4.666 ± 0.086 (> 10.7) | 36.000 ± 1.150 (> 1.3) | > 50.000 ± 1.541 | | |
| 17p | 5.512 ± 0.138 (2.6) | 7.316 ± 0.226 (1.9) | 5.430 ± 0.140 (2.6) | 12.990 ± 0.284 (1.1) | 14.200 ± 0.638 | | |
| 17q | 11.760 ± 0.400 (2.3) | 13.360 ± 0.325 (2.0) | 9.134±0.314 (3.0) | 24.510 ± 0.204 (1.1) | 27.200 ± 0.813 | | |
| 17r | 7.670 ± 0.379 (2.2) | 8.292 ± 0.497 (2.1) | 6.224 ± 0.082 (2.7) | 14.180 ± 0.135 (1.2) | 17.020 ± 0.557 | | |
| 17s | 5.416 ± 0.288 (1.9) | 6.134 ± 0.131 (1.7) | 4.639 ± 0.068 (2.2) | 8.096 ± 0.091 (1.3) | 10.200 ± 0.545 | | |
| 17t | 7.342 ± 0.161 (3.5) | 9.474 ± 0.097 (2.7) | 6.447 ± 0.111 (3.9) | 14.120 ± 0.201 (1.8) | 25.350 ± 0.951 | | |
| Sunitinibb | 9.67 | 16.91 | 3.97 | - | - | | |
| 5-Fluorouracil ^{b,c} | 20.43 | - | 3.15 | - | - | | |
| Doxorubicin ^c | - | _ | - | 5.93 | - | | |

 $\begin{tabular}{ll} \textbf{Table 1}. & Antiproliferation properties of the tested compounds. aSI = Selectivity index (IC_{50} of RPE1 "normal cell"/IC_{50} of cancer cell), bReference 30, cReference 45. \\ \end{tabular}$

Chlorophenyl is preferable than the fluorophenyl as anti-HCT116, anti-PaCa2, anti-MCF7, and anti-A549
 Methyphenyl has better anti-HCT116 properties than the 4-methoxyphenyl

Fig. 6. Summary of the most important items revealed through analysis of SARs due to antiproliferation properties of 17a-t against the tested cancer cell lines.

17g (R=4-FC₆H₄, R'=Me), 17h (R=4-ClC₆H₄, R'=H), 17l (R=4-BrC₆H₄, R'=H), 17o (R=4-H₃CC₆H₄, R'=Cl), and 17s (R=2-thienyl, R'=Cl), exhibit considerable potencies (IC₅₀=6.092-6.354 μ M).

SAR based on the observed anti-PaCa2 properties indicate that the 5-chloroindolyl bearing compounds have higher anti-PaCa2 activity than that of the 5-fluoroindolyl-containing analogs as seen in pairs 17c/17b (IC $_{50}$ =9.148/12.230 µM, respectively), 17j/17i (IC $_{50}$ =6.930/13.450 µM, respectively), 17o/17n (IC $_{50}$ =6.273/15.340 µM, respectively), and 17s/17r (IC $_{50}$ =6.134/8.292 µM, respectively) (Fig. 6).

MCF7 Breast cancer is the second highest cause of malignant mortality in women. According to the National Breast Cancer Coalition, one woman dies due to this disease every 13 min globally. It is a heterogeneous disease that is difficult to diagnose, especially in the early stages. Although several techniques have been developed and are clinically used (including, X-ray, ultrasound, computed tomography (CT), and magnetic resonance imaging), low sensitivity and specificity is a challenge impacting these tools. Patients with less than 1 cm³ (about 10° cancer cells) usually return negative imaging results. This is a serious challenge, not only for the diagnosis but also for the treatment, that needs highly effective agents with minimal drawbacks^{54,55}.

Compound 17j (R=4-ClC $_6$ H $_4$, R'=Cl) is the most promising agent synthesized (IC $_{50}$ = 3.874 μ M) with anti-MCF7 potency close to that of 5-fluorouracil (a clinically usable drug agent with IC $_{50}$ = 3.15 μ M). Compounds 17h (R=4-ClC $_6$ H $_4$, R'=H), 17m (R=4-H $_3$ CC $_6$ H $_4$, R'=H), and 17n (R=4-H $_3$ CC $_6$ H $_4$, R'=F) also exhibit anti-MCF7 properties (IC $_{50}$ = 4.067-4.368 μ M) close to that of 5-fluorouracil. Based on the anti-MCF7 properties of the synthesized compound 17a-t, some SARs were noted that seem similar to those for anti-HCT116 agents. The 4-chlorophenyl-containing compounds are superior among all the halogenated phenyl-containing analogs (fluoro or bromo derivatives) as shown by compounds 17h/17e/17l (IC $_{50}$ = 4.067/5.640/4.852 μ M, respectively), 17j/17f (IC $_{50}$ =3.874/5.289 μ M, respectively), and 17k/17g (IC $_{50}$ =4.978/5.426 μ M, respectively). The 5-chloroindolyl-containing compounds have more enhanced anti-MCF7 properties than the 5-fluoroindolyl analogs (compound 17o is an exception), as noted for compounds 17c/17b (IC $_{50}$ =5.269/5.826 μ M, respectively), 17j/17i (IC $_{50}$ =3.874/4.808 μ M, respectively), and 17s/17r (IC $_{50}$ =4.639/6.224 μ M, respectively) (Fig. 6).

A549 Lung cancer is one of the most prevalent and deadly types of cancer (with a low five-year survival rate of 15%), due to difficulties in early detection as it is usually asymptomatic⁵⁶. Metastasis and recurrence of this disease are major factors contributing to the low survival rate. Tobacco smoking, unhealthy environmental conditions and genetic elements are linked to lung cancer⁵⁷. Two main types of lung cancers have been identified, non-small cell cancer which is the most common (85%), and small cell lung cancer (15%), which is more aggressive⁵⁸.

Compound 17h (R=4-ClC₆H₄, R'=H; IC₅₀=4.149 μ M) is the most effective anti-A549 analog, surpassing doxorubicin (IC₅₀=5.93 μ M). Additionally, compounds 17j (R=4-ClC₆H₄, R'=Cl), and 17k (R=4-ClC₆H₄, R'=Me) also show high efficacies (IC₅₀=6.059, 6.467 μ M, respectively).

SARs derived from the observed anti-A549 properties mirror those noted for other cancer cell lines (HCT116, MCF7). The 4-chlorophenyl group is preferable over the other 4-halogenated phenyl residues as shown by compounds 17h/17e/17l (IC $_{50}$ =4.149/7.727/7.281 μ M, respectively), 17j/17f (IC $_{50}$ =6.059/>50.000 μ M, respectively), and 17k/17g (IC $_{50}$ =6.467/8.149 μ M, respectively). 5-Chloroindolyl-containing compounds have more enhanced anti-A549 properties than the 5-fluoroindolyl-containing analogs (17b is an exception), as illustrated by compounds 17j/17i (IC $_{50}$ =6.059/>50.000 μ M, respectively), 17o/17n (IC $_{50}$ =36.000/>50.000 μ M, respectively), and 17s/17r (IC $_{50}$ =8.096/14.180 μ M, respectively) (Fig. 6).

Some of the synthesized agents showed a high selectivity index (SI) due to IC_{50} values against RPE1 (healthy/non-cancer) compared to the tested cancer cell line(s) including 17f, 17i, 17j, 17n, and 17o. However, these

| Compd | %CT (± SEM) |
|-------|-------------|
| 17d | 64.1 ± 7.0 |
| 17k | 53.1 ± 2.2 |
| 17p | 68.3 ± 0.6 |
| 17s | 77.9 ± 1.2 |

Table 2. The percentage cytotoxicity (%CT) of the effective agents against HCT116 3D-spheroid at 50 μM.

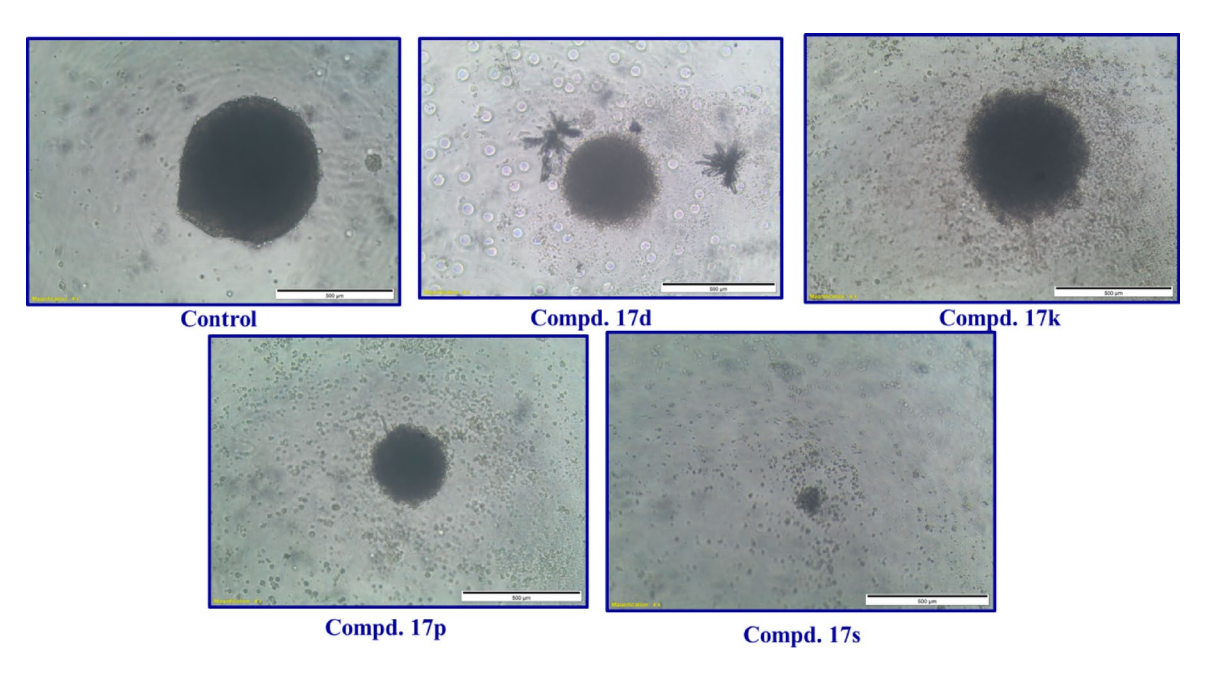


Fig. 7. HCT116 3D-multilayer spheroids contained proliferating control and treated with 50 μ M of compounds 17d, 17k, 17p, and 17s.

preliminary observations are only indicative based on cell line testing and the most important data come from further biological studies, such as animal modeling.

3D-multicellular spheroid

The 3D-multicellular spheroid model is an important technique bridging and/or linking the biological properties of a specific agent, shown to have a promising antiproliferation effect in the in vitro 2D-single layer culture, with the in vivo animal model. This is due to the physiological environment available in the 3D-spheroid that allows cell-cell interactions, due to their morphological capacity, with similarity to that of cancer tissue. Oxygen and nutrient transmission in the 3D-multilayer model is highly similar to that of the in vivo tissue. In contrast, cells in the 2D-single layer technique possess sufficient nutrients and oxygen allowing high proliferation rates relative to the 3D-technique. Additionally, drug penetration to the inner cell layers of the spheroid is more difficult thus allowing high survival rates for the inner layers than the outer ones. This makes the 3D-spheroid technique a close mimic platform to in vivo modeling 59,60.

The synthesized agents were subjected to 3D-multilayer HCT116 cancer spheroid utilizing the standard methodology 61,62 . From the observed results it is noted that, some of the synthesized agents reveal promising activity at 50 μ M (Table 2, Fig. 7). Compound 17s (R=2-thienyl, R'=Cl) is the most promising agent noted revealing antiproliferation properties of 77.9% relative to the control experiment. Compounds 17p (R=4-H_3COC_6H_4, R'=H), and 17d (R=Ph, R'=Me) show slightly lower efficacies (%CT=68.3, and 64.1, respectively) and compound 17k (R=4-ClC_6H_4, R'=Me) has even milder properties (%CT=53.1).

Biochemical studies

VEGFR-2 inhibitory properties

VEGFR-2 inhibitory properties of the synthesized agents 17a-t were determined by the standard technique 63 at 10 μ M against HCT116, MCF7, and PaCa2 cancer cells and compared with the standard reference, sunitinib (Table 3, Figs. 8 and 9).

HCT116 Synthesized agents 17p (R=4-H₃COC₆H₄, R'=H) and 17a (R=Ph, R'=H) revealed high VEG-FR-2 inhibitory properties at 10 μM against HCT116 cancer cells with higher efficacies (% inhibition=90.0 and 88.0, respectively) than that of the standard reference sunitinib (% inhibition=87.9). Agents 17c (R=Ph,

| | HCT116 | | PaCa2 | | MCF7 | |
|-----------|--------------|--------------|--------------|--------------|--------------|--------------|
| Compd | pg/mL±SEM | % Inhibition | pg/mL±SEM | % Inhibition | pg/mL±SEM | % Inhibition |
| 17a | 38.20 ± 1.6 | 88.0 | 19.26 ± 1.0 | 94.1 | 51.50 ± 0.8 | 80.1 |
| 17b | 73.25 ± 2.0 | 77.0 | 38.75 ± 1.4 | 88.1 | 77.20 ± 0.6 | 70.2 |
| 17c | 44.50 ± 1.1 | 86.0 | 28.43 ± 1.0 | 91.3 | 60.40 ± 0.5 | 76.7 |
| 17d | 87.40 ± 1.9 | 72.5 | 53.42 ± 0.7 | 83.7 | 72.80 ± 1.2 | 71.9 |
| 17e | 107.50 ± 2.0 | 66.2 | 127.43 ± 1.3 | 61.0 | 116.50 ± 1.0 | 55.0 |
| 17f | 43.70 ± 0.9 | 86.2 | 27.53 ± 1.1 | 91.6 | 63.20 ± 0.9 | 75.6 |
| 17g | 98.40 ± 1.2 | 69.0 | 72.80 ± 0.9 | 77.7 | 64.80 ± 0.5 | 75.0 |
| 17h | 51.74 ± 1.5 | 83.7 | 18.25 ± 0.6 | 94.4 | 52.70 ± 0.7 | 79.6 |
| 17i | 81.40 ± 1.9 | 74.4 | 42.76 ± 0.7 | 86.9 | 49.50 ± 0.3 | 80.9 |
| 17j | 62.50 ± 0.7 | 80.3 | 24.78 ± 0.3 | 92.4 | 44.80 ± 0.6 | 82.7 |
| 17k | 67.80 ± 1.3 | 78.7 | 76.40 ± 0.9 | 76.6 | 86.40 ± 0.5 | 66.6 |
| 17l | 84.20 ± 1.5 | 73.5 | 86.45 ± 1.2 | 73.5 | 73.50 ± 0.8 | 71.6 |
| 17m | 44.50 ± 0.5 | 86.0 | 25.36 ± 1.0 | 92.2 | 42.80 ± 0.4 | 83.5 |
| 17n | 115.30 ± 2.2 | 63.7 | 40.70 ± 1.6 | 87.5 | 85.60 ± 0.7 | 66.9 |
| 17o | 48.40 ± 0.6 | 84.8 | 31.64±1.9 | 90.3 | 38.70 ± 0.4 | 85.0 |
| 17p | 31.80 ± 0.8 | 90.0 | 21.76±0.4 | 93.3 | 48.30 ± 0.4 | 81.3 |
| 17q | 132.30 ± 0.9 | 58.4 | 135.70 ± 1.7 | 58.5 | 145.70 ± 1.9 | 43.7 |
| 17r | 67.34 ± 0.4 | 78.8 | 66.53 ± 0.8 | 79.6 | 84.30 ± 1.0 | 67.4 |
| 17s | 53.80 ± 0.9 | 83.1 | 26.50 ± 0.5 | 91.9 | 47.60 ± 0.6 | 81.6 |
| 17t | 124.70 ± 1.3 | 60.8 | 115.00 ± 0.9 | 64.8 | 96.70 ± 1.2 | 62.6 |
| Sunitinib | 38.50 ± 1.0 | 87.9 | 45.30 ± 0.2 | 86.1 | 48.70 ± 1.0 | 81.2 |
| Control | 317.80 ± 3.5 | - | 326.80 ± 1.9 | - | 258.70 ± 2.3 | - |

Table 3. The percentage VEGFR-2 inhibitory properties of the tested compounds at $10 \mu M$.

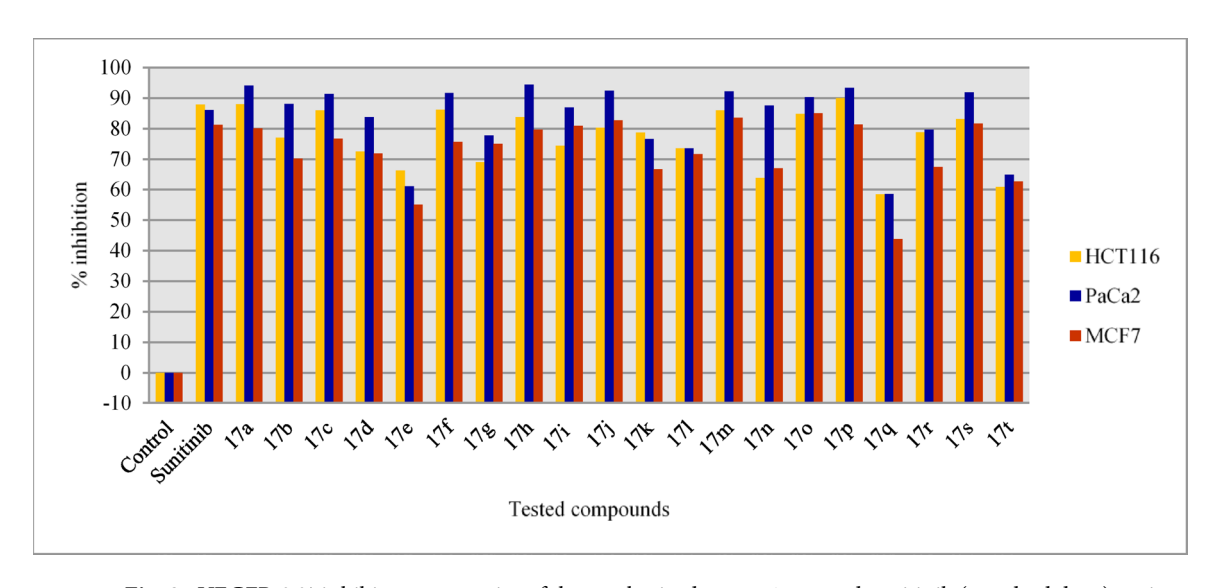


Fig. 8. VEGFR-2 % inhibitory properties of the synthesized agents 17a-t and sunitinib (standard drug) against HCT116, PaCa2, and MCF7 cancer cells.

R'=Cl), 17f (R=4-FC₆H₄, R'=Cl), and 17m (R=4-H₃CC₆H₄, R'=H) also showed biochemical properties (% inhibition = 86.2- 86.0) close to that of sunitinib. Compounds 17h (R=4-ClC₆H₄, R'=H), 17o (R=4-H₃CC₆H₄, R'=Cl), and 17s (R=2-thienyl, R'=Cl) also had considerable VEGFR-2 inhibitory effect (% inhibition = 84.8-83.1).

SAR based on the observations indicated that the 5-chloroindolyl heterocycle is preferable to fluoro or methyl derivatives for VEGFR-2 inhibition as noted in analogs 17c/17b/17d (% inhibition=86.0/77.0/72.5), 17f/17g (% inhibition=86.2/69.0), 17j/17i/17k (% inhibition=80.3/74.4/78.7), 17o/17n (% inhibition=84.8/63.7), and 17s/17r/17t (% inhibition=83.1/78.8/60.8).

Fig. 9. Summary of the most important items revealed through analysis of SARs due to VEGFR-2 inhibitory properties of 17a-t utilizing the lysate of the tested cancer cell lines.

<u>PaCa2</u> Some of the synthesized agents [17a (R=Ph, R'=H), 17h (R=4-ClC₆H₄, R'=H), and 17p (R=4-H₃COC₆H₄, R'=H, % inhibition=94.4-93.3) are with distinguished anti-VEGFR-2 properties higher than that of sunitinib (% inhibition=86.1) upon testing on PaCa2 cancer cells at 10 μ M. Promising anti-VEGFR-2 properties (% inhibition=92.4-90.3) are also noted by compounds 17c (R=Ph, R'=Cl), 17f (R=4-FC₆H₄, R'=Cl), 17m (R=4-H₃CC₆H₄, R'=H), 17o (R=4-H₃CC₆H₄, R'=Cl), and 17s (R=2-thienyl, R'=Cl).

SAR based on the observed anti-VEGFR-2 properties evidenced the importance of the chloro substituent linked at the 5-position of the indolyl heterocycle relative to the fluoro and methyl substitution for the anti-VEGFR-2 properties enhancement as noted in analogs 17c/17b/17d (% inhibition=91.3/88.1/83.7), 17f/17g (% inhibition=91.6/77.7), 17j/17i/17k (% inhibition=92.4/86.9/76.6), 17o/17n (% inhibition=90.3/87.5), and 17s/17r/17t (% inhibition=91.9/79.6/64.8).

MCF7 Agents 17ο (R=4-H $_3$ CC $_6$ H $_4$, R'=Cl), 17m (R=4-H $_3$ CC $_6$ H $_4$, R'=H), and 17j (R=4-ClC $_6$ H $_4$, R'=Cl) have VEGFR-2 inhibitory effects (% inhibition=85.0, 83.5, and 82.7, respectively) higher than that of the standard drug (sunitinib, % inhibition=81.2) at 10 μM in breast cancer cell (MCF7). Compounds 17s (R=2-thienyl, R'=Cl), and 17p (R=4-H $_3$ COC $_6$ H $_4$, R'=H) also have high efficacies (% inhibition=81.6, 81.3). Other analogs, including 17i (R=4-ClC $_6$ H $_4$, R'=F), and 17a (R=Ph, R'=H), also have close inhibitory effect (% inhibition=80.9, 80.1) to that of sunitinib.

SAR noted from the anti-VEGFR-2 properties show the favorable effect of chloro substituent of the indolyl heterocycle relative to the fluoro or methyl substituents as seen in analogs 17c/17b/17d (% inhibition=76.7/70.2/71.9), 17f/17g (% inhibition=75.6/75.0), 17j/17i/17k (% inhibition=82.7/80.9/66.6), 17o/17n (% inhibition=85.0/66.9), and 17s/17r/17t (% inhibition=81.6/67.4/62.6). From these observations, it is clear that the attachment of a chloro substituent to the indolyl heterocycle at the 5-position enhances anti-VEGFR-2 properties relative to other elements/group (fluoro or methyl) in MCF7 in common with the other tested cell lines (HCT116 and PaCa2).

COX-1/-2 inhibitory properties

Cyclooxygenases (COXs) are enzymes involved in the production of important bio-mediators including prostaglandins from arachidonic acid. Two main forms have been identified, COX-1 (expressed in many tissues with many biological functions including in gastric mucosa and kidney), and COX-2 (inducible during inflammation). Several non-steroidal anti-inflammatory drugs (NSAIDs) with COX inhibition have been discovered and clinically recommended for inflammation and pain symptoms. Few of them are known with selectivity towards COX- 2^{64} . Previous publications have mentioned the anti-inflammatory properties of both natural⁶⁵, and synthetic spiro-indolin-2-ones⁶⁶. Many reports have described the linkage between inflammation and some cancer types⁶⁷. Some inflammatory mediators such as TNF- α (tumor necrosis factor- α)^{68,69}, IL-6 (interleukin-6)^{70,71}, and COX- $2^{72,73}$ are also involved in cancer initiation, invasion, and development.

The synthesized agents 17a-t were tested for COX-1/-2 activity by the standard techniques 74,75 and compared with the known NSAIDs (ibuprofen and indomethacin) (Table 4). Compound 17g (R=4-FC₆H₄, R'=Me) is the most promising agent against COX-1 (% inhibition=62.1) with slightly lower efficacy than the standard NASIDs (% inhibition=65.3 and 64.3 for ibuprofen and indomethacin, respectively). Close efficacies were also noted for compounds 17l (R=4-BrC₆H₄, R'=H), 17o (R=4-H₃CC₆H₄, R'=Cl), and 17q (R=2-thienyl, R'=H) (% inhibition=61.7-61.3).

Compound 17a (R=Ph, R'=H) is the most promising agent against COX-2 (% inhibition=64.9) being closest to the NSAIDs (% inhibition=71.3 and 68.3 for ibuprofen and indomethacin, respectively). Notable properties are also observed for compounds 17t (R=2-thienyl, R'=Me), 17q (R=2-thienyl, R'=H), and 17b (R=Ph, R'=F) (% inhibition=63.7-61.3). Slight enhancement of selectivity index (SI, COX-2/COX-1) was noted for 17k, and 17t (SI=1.30 and 1.29, respectively), relative to the NSAIDs (SI=0.95 and 1.09 for ibuprofen and indomethacin, respectively).

TNF- α inhibitory properties

TNF- α is an important cytokine auto-produced by the immune system in association with different disorders including inflammation and cancer^{76–79}. Concentration of TNF- α can be a therapeutic indicator for many diseases associated with inflammation and infectious diseases^{80–82}. The synthesized compounds 17a-t within the current study were assessed for TNF- α inhibitory properties by the standard technique and compared

| Compd | % Inhibition of COX-1 ± SEM | % Inhibition of COX-2±SEM | SI |
|--------------|-----------------------------|---------------------------|------|
| 17a | 49.8 ± 1.8 | 64.9 ± 2.8 | 0.96 |
| 17b | 53.7 ± 3.7 | 61.3 ± 2.6 | 1.04 |
| 17c | 58.6 ± 3.5 | 53.9 ± 1.7 | 1.05 |
| 17d | 51.8 ± 2.2 | 56.4±1.9 | 0.82 |
| 17e | 55.0 ± 3.6 | 59.6 ± 1.3 | 1.08 |
| 17f | 57.6 ± 1.1 | 60.8 ± 2.7 | 1.01 |
| 17g | 62.1 ± 3.1 | 51.8 ± 2.8 | 0.96 |
| 17h | 53.5 ± 2.8 | 51.5±3.1 | 1.06 |
| 17i | 46.2 ± 2.4 | 49.7 ± 1.9 | 1.09 |
| 17j | 48.9 ± 1.5 | 53.5 ± 2.3 | 1.05 |
| 17k | 57.7 ± 1.0 | 55.0 ± 1.6 | 1.30 |
| 17l | 61.6 ± 1.2 | 50.3 ± 2.3 | 0.92 |
| 17m | 58.3 ± 3.0 | 60.9 ± 1.1 | 0.93 |
| 17n | 50.6 ± 2.3 | 47.3 ± 1.4 | 1.08 |
| 17o | 61.7 ± 3.4 | 59.3 ± 2.4 | 1.14 |
| 17p | 51.1 ± 2.7 | 53.5 ± 2.1 | 1.10 |
| 17q | 61.3 ± 1.5 | 62.1 ± 3.1 | 0.93 |
| 17r | 55.5 ± 2.6 | 51.8 ± 2.0 | 1.09 |
| 17s | 53.8 ± 2.8 | 56.3 ± 2.3 | 0.83 |
| 17t | 49.2 ± 1.9 | 63.7 ± 1.7 | 1.29 |
| Ibuprofen | 65.3 ± 1.2 | 71.3 ± 1.8 | 0.95 |
| Indomethacin | 64.3 ± 2.7 | 68.3 ± 1.6 | 1.09 |

Table 4. COX-1/-2 inhibitory properties of the tested agents at 10 μ M.

with those of NSAIDs (ibuprofen, and indomethacin) 83 . The results show that some of the synthesized agents have more promising inhibitory properties towards TNF- α relative to the standard drug used (Table 5). Compound 17h (R=4-ClC₆H₄, R'=H) is the most effective analog noted for HCT116 cell lysate (% inhibition at 10 μ M=80.7, 22.2 and 42.8, for 17h, ibuprofen and indomethacin; i.e. 3.6- and 1.9-fold the standards, respectively). Compounds 17m and 17a also show considerable biological properties (% inhibition=77.4 and 74.0, respectively). Other synthesized agents with promising activity but with lower efficacies are 17i, 17k, 17l, 17p, and 17r (% inhibition=72.6-70.2).

Compound 17i (R=4-ClC₆ H_4 , R'=F) is the most effective agent upon testing with PaCa2 cell lysate (% inhibition=79.6, 42.0 and 32.6 for 17i, ibuprofen and indomethacin; i.e. 1.9- and 2.4-fold the standards, respectively). Compounds 17a, 17 h, 17k, and 17p also reveal high TNF- α inhibitory properties (% inhibition=78.3-76.3).

The synthesized agent 17a (R = Ph, R' = H) is the most promising agent observed upon assessment with MCF7 cell lysate (% inhibition = 78.1, 7.8 and 22.9 for 17a, ibuprofen and indomethacin, respectively). Compounds 17h, and 17b also exhibit promising activities (% inhibition = 74.0 and 72.2, respectively).

Chick chorioallantoic membrane (CAM) studies

CAM assay is an established xenograft technique for investigating the angiogenic effect due to the high resemblance of the human vascularized epithelium basement membrane with that of the chorioallantoic layer containing mainly type IV collagen^{84–86}. Some of the promising anti-VEGFR-2 agents (17a, 17i, 17m, 17p, and 17s) were subjected for CAM testing studies and compared with that of sunitinib²³ (a potent drug with VEGFR-2 inhibitory effect) (Table 6, Figs. 10 and 11). The results show that synthesized agent 17s (R=2-thienyl, R'=Cl) exhibits inhibitory effect in the CAM test (% inhibition=86.7) close to that of the standard drug sunitinib (% inhibition=88.6) which is consistent with its anti-VEGFR-2 properties relative to the standard drug tested (% anti-VEGFR-2 inhibition=83.1/87.9, 81.6/81.2 and 91.9/86.1 for 17 s/sunitinib against HCT116, MCF7, and PaCa2 cancer cell lines, respectively). Promising anti-angiogenic properties (% inhibition=82.7-81.4) from the CAM test were also observed for compounds 17p (R=4-H₃COC₆H₄, R'=H), 17a (R=Ph, R'=H), and 17m (R=4-H₃CC₆H₄, R'=H), consistent with the anti-VEGFR-2 properties (% anti-VEGFR-2 inhibition=90.0/88.0/86.0, 81.3/80.1/83.5, 93.3/94.1/92.2 for HCT116/MCF7/ PaCa cancer cells, respectively). It should also be noted that the small differences between the antiproliferation, anti-VEGFR-2, and anti-angiogenic properties (Tables 1, 3, and 4) are attributable to the conditions applied for each procedure/ protocol utilizing either human cell lines, kit enzyme, or xenograft model.

QSAR studies

QSAR (quantitative SAR) is a computational chemical methodology useful not only for predicting biological properties quantitatively but also for determining the controlling functions and/or properties of biological active entities. Many medicinal chemical studies, including CODESSA-Pro software have described the successful utilization of this methodology ^{87,88}.

| | HCT116 | | PaCa2 | | MCF7 | |
|--------------|---------------|--------------|---------------|--------------|---------------|--------------|
| Compd | pg/mL (± SEM) | % inhibition | pg/mL (± SEM) | % inhibition | pg/mL (± SEM) | % inhibition |
| 17a | 24.86 ± 0.8 | 74.0 | 24.8 ± 1.5 | 77.8 | 18.25 ± 1.1 | 78.1 |
| 17b | 94.64 ± 2.2 | 1.1 | 105.7 ± 3.9 | 5.5 | 82.25 ± 2.6 | 1.2 |
| 17c | 31.72 ± 1.2 | 66.9 | 33.8 ± 2.2 | 69.8 | 23.16 ± 0.7 | 72.2 |
| 17d | 94.80 ± 2.5 | 1.0 | 103.7 ± 4.2 | 7.2 | 83.2 ± 4.5 | 0.1 |
| 17e | 94.27 ± 0.7 | 1.5 | 97.6 ± 1.6 | 12.7 | 81.87 ± 3.0 | 1.7 |
| 17f | 85.46 ± 1.3 | 10.7 | 109.8 ± 4.7 | 7.2 | 82.45 ± 4.0 | 1.0 |
| 17g | 81.75 ± 2.1 | 14.6 | 97.4±3.6 | 12.9 | 83.0 ± 3.2 | 0.3 |
| 17h | 18.45 ± 1.1 | 80.7 | 26.5 ± 0.7 | 76.3 | 21.65 ± 3.1 | 74.0 |
| 17i | 28.56 ± 0.9 | 70.2 | 22.8 ± 1.6 | 79.6 | 31.27 ± 1.3 | 62.4 |
| 17j | 81.78 ± 1.4 | 14.6 | 98.5 ± 3.1 | 11.9 | 82.87 ± 4.5 | 0.5 |
| 17k | 26.48 ± 1.5 | 72.3 | 24.3 ± 1.4 | 78.3 | 22.85 ± 1.8 | 72.6 |
| 17l | 27.34 ± 1.1 | 71.4 | 37.63 ± 0.8 | 66.3 | 33.67 ± 1.7 | 59.6 |
| 17m | 21.65 ± 0.9 | 77.4 | 32.83 ± 1.3 | 70.6 | 26.24 ± 2.2 | 68.5 |
| 17n | 86.47 ± 2.4 | 9.7 | 96.3 ± 3.0 | 13.9 | 83.17 ± 4.1 | 0.1 |
| 17o | 86.34 ± 0.9 | 9.8 | 95.6 ± 2.2 | 14.5 | 81.85 ± 3.1 | 1.7 |
| 17p | 26.21 ± 1.3 | 72.6 | 25.8 ± 1.8 | 76.9 | 28.56 ± 2.9 | 65.7 |
| 17q | 84.26 ± 0.8 | 12.0 | 91.8 ± 2.7 | 17.9 | 80.67 ± 2.8 | 3.1 |
| 17r | 27.45 ± 1.4 | 71.3 | 27.5 ± 0.5 | 75.4 | 25.46 ± 0.9 | 69.4 |
| 17s | 86.57 ± 2.0 | 9.6 | 90.6 ± 2.8 | 19.0 | 81.64±3.7 | 1.9 |
| 17t | 81.64 ± 2.1 | 14.7 | 95.8 ± 2.5 | 14.3 | 82.91 ± 3.8 | 0.4 |
| Ibuprofen | 74.5 ± 1.1 | 22.2 | 64.8 ± 0.6 | 42.0 | 76.8 ± 2.0 | 7.8 |
| Indomethacin | 54.8 ± 0.7 | 42.8 | 75.3 ± 2.1 | 32.6 | 64.2 ± 1.6 | 22.9 |
| Control | 95.74±0.5 | - | 111.8 ± 2.0 | - | 83.26 ± 1.1 | - |

Table 5. TNF- α inhibitory properties of the tested agents at 10 μ M.

| Compd | Diameter of blood vessel (μm±SEM) | % Inhibition |
|-----------|-----------------------------------|--------------|
| Control | 459.7 ± 13.8 | - |
| Sunitinib | 52.3 ± 1.7 | 88.6 |
| 17a | 80.7 ± 3.7 | 82.5 |
| 17i | 219.3 ± 5.6 | 52.3 |
| 17m | 85.7 ± 2.6 | 81.4 |
| 17p | 79.3 ± 3.3 | 82.7 |
| 17s | 61.3 ± 4.3 | 86.7 |

Table 6. % inhibitory properties of the blood vessels by the tested compound in CAM test.

HCT116

A robust four descriptor QSAR model (R^2 =0.954, R^2 cvOO=0.901, R^2 cvMO=0.911) was obtained for the anti-HCT116 training set compounds (17a-e, g-s, representing 90% of the synthesized agents) (Supplementary Tables S2-S5, Fig. S30). Compounds 17f and 17t (IC_{50} =3.716 and 7.342 μ M, of potent and mild anti-HCT116 efficacies, respectively) were used as external test set analogs for validating the observed model. The QSAR model covers a wide range of anti-HCT116 properties [log IC_{50} (observed: 0.488551-1.07041, predicted: 0.490357-1.07339) μ M] including potent and mild effective agents. Complementary information content (t "criterion value" = 7.792) is a topological descriptor with low coefficient value = 0.005. However, due to the high descriptor value of some respective analogs, a potential effect is noted for the predicted anti-HCT116 properties as shown in compounds 17d/17s (descriptor value = 220.206/150.022, estimated IC_{50} = 9.892/5.803 μ M). Complementary information content can be calculated by equations (S1,S2)⁸⁹.

The bond order for atom O is a semi-empirical descriptor (t=5.685) with the highest coefficient value (13.0248) among all the model's descriptors. This can justify the estimated anti-HCT116 values of compounds 17b/17h (descriptor value = 0.145/0.136, estimated anti-HCT116 IC₅₀ = 8.233/3.302 μ M).

Repulsion energy between two different atoms (C-N) is a semi-empirical descriptor with coefficient value = 0.353. Compound with high mathematical descriptor value gives rise to low anti-HCT116 predicted properties as noted in compounds 17d/17m (descriptor value = 168.125/167.772, estimated anti-HCT116 IC₅₀ = $9.892/3.932~\mu$ M). The nuclear repulsion energy between two different atoms can be calculated by equation (S3)⁸⁹.

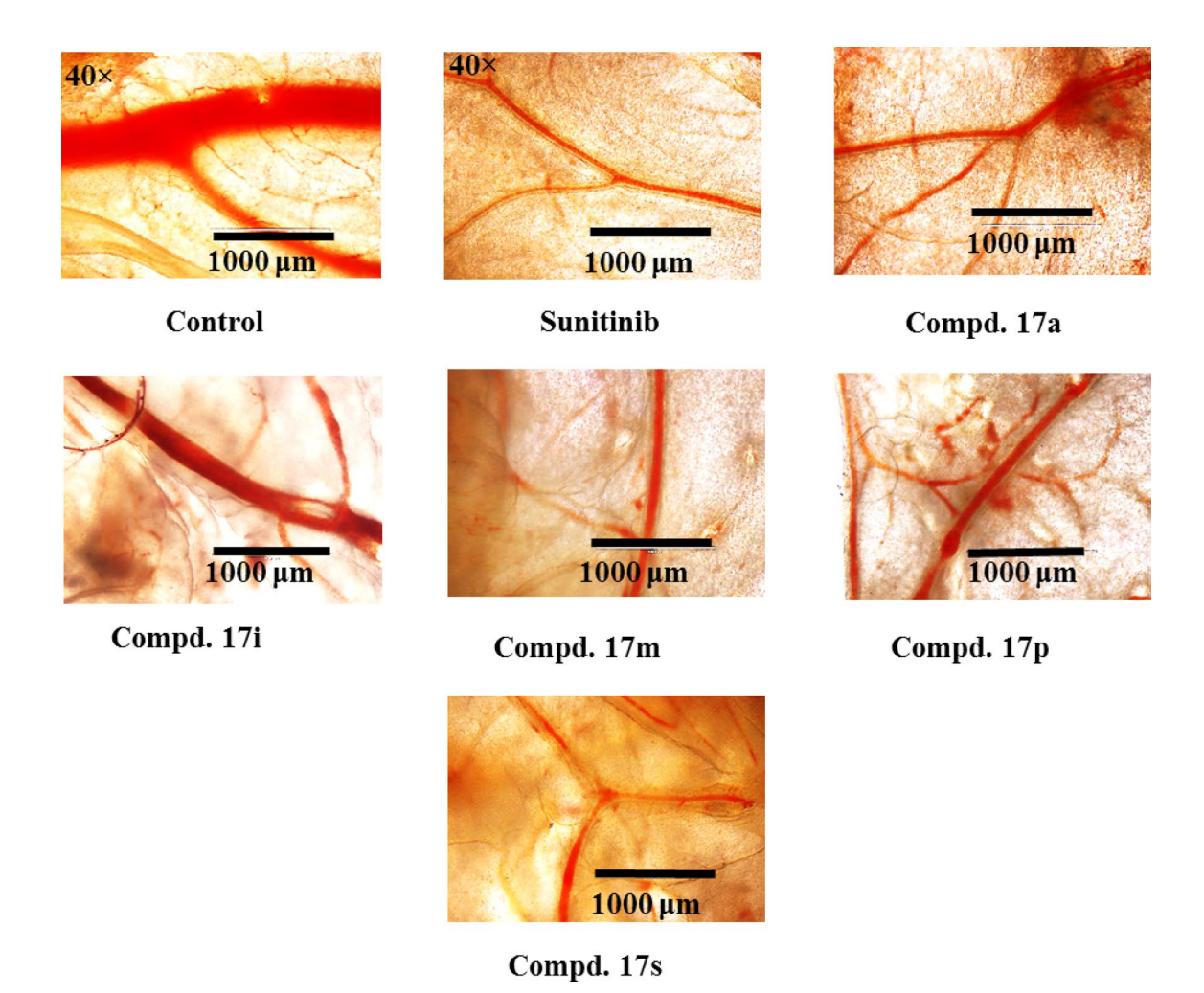


Fig. 10. Images of light microscopy for anti-angiogenic evaluation of the tested compounds using CAM assay. A total amount of 20 μ L (end concentration of 660 μ M) of sunitinib and tested compounds were pipetted on glass slide and left to dry. The glass slide was placed on the surface of the CAM blood vessel network and left in an incubator at 37 °C for 3 days. The CAM blood vessel network was carefully cut and imaged under a light microscope (40 × magnification).

Molecular volume is a geometrical descriptor with indication for the ability of a specific agent to be fitted in the protein/receptor active site so, revealing a potential bio-activity. It possesses a coefficient value with a negative sign (-0.010). So, analog(s) with high mathematical value can predicate a potent estimated anti-HCT116 effect as noted in compounds 17a/17o (descriptor value=531.584/576.648, estimated anti-HCT116 $IC_{50}=7.039/3.728~\mu M$). Molecular volume of an agent can be calculated by equation (S4)⁸⁹.

<u>PaCa2</u> A training set containing 17a,c-g,i-t (18 compounds out of 20 synthesized analogs of potential anti-PaCa2 properties) was used for optimizing a QSAR model. A validated 4-descriptor QSAR model was obtained (R^2 =0.959, R^2 cvOO=0.927, R^2 cvMO=0.930) covering a considerable range of anti-PaCa2 properties [1/ IC₅₀ (observed: 0.064-0.1904, predicted: 0.067-0.190) μ M). Two of the synthesized analogs 17b and 17h were used as external test set compounds representing mild and promising anti-PaCa2 agents (Supplementary Tables S6-S9, Fig. S31).

Rotational entropy is a thermodynamic descriptor (coefficient = 0.078). Analog(s) with high mathematical value can estimate high anti-PaCa2 properties due to $1/IC_{50}$ model assigned as noted in compounds 17 l/17q (descriptor value = 39.663/37.669, estimated IC_{50} = 5.952/13.873 μ M). The rotational entropy can be calculated by equation (S5)⁸⁹.

Resonance energy between two different atoms is a semi-empirical descriptor with coefficient value = 0.293, explaining the anti-PaCa2 properties of analogs 17a/17o (descriptor value=17.469/17.782, estimated $IC_{50} = 13.639/6.358 \,\mu\text{M}$). Equation (S6) can calculate the resonance energy between two different atoms⁸⁹.

Total interaction energy between two different atoms is also a semi-empirical descriptor with coefficient value = 0.115, evidencing the estimated anti-PaCa2 properties of compounds 17d/17t (descriptor value = 12.388/12.969, estimated $IC_{50} = 15.024/9.106 \mu M$). The descriptor values can be calculated by equation (S7)⁸⁹.

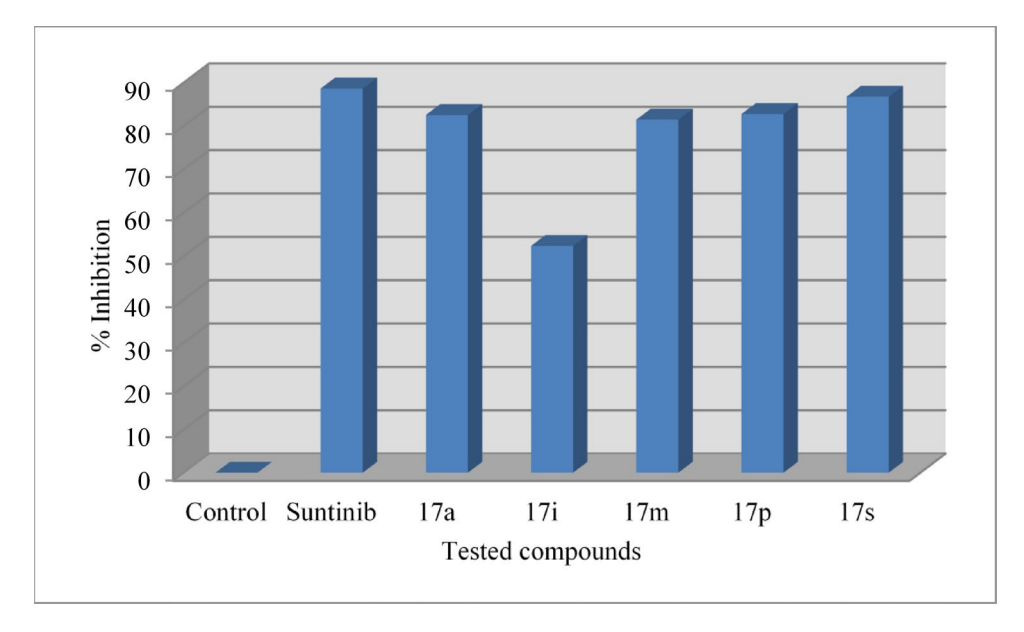


Fig. 11. % inhibition of angiogenic effect of the tested compounds (17a, 17i, 17m, 17p, and 17s), and sunitinib (reference drug) using CAM assay.

Shadow plane XY is a geometrical descriptor with a negative sign coefficient value (-0.003). Compounds with high mathematical value can estimate low anti-PaCa2 properties due to $1/IC_{50}$ modeling. This is noted in compounds 17i/17s (descriptor value = 139.24/102.38, estimated IC_{50} = 13.581/7.735 μ M). Equation (S8) can calculate the shadow area of a specific molecule⁸⁹.

Internal and external validations The estimated antitumor properties relative to the noted experimental activities are the main internal validation elements evidencing the robust QSAR models obtained. Statistical values including leave-one-out and leave-many-out coefficients relative to the main coefficient value of the observed models (R^2 =0.954/0.959, R^2 cvOO=0.901/0.927, R^2 cvMO=0.911/0.930 for HCT116/PaCa2 models, respectively) are also important evidence for the goodness of the QSAR models. The standard deviation (s^2) compare to Fisher criteria (F) are also important evidences for the robust QSAR models (s^2 =0.002/9.373e-005, F=67.611/75.400 for HCT116/PaCa2 models, respectively).

External validation of the QSAR models was undertaken considering a potent and a mild antitumor agent (17f/17t, 17b/17h, for HCT116 and PaCa2 models, respectively). The estimated biological properties relative to the observed ones (estimate IC $_{50}$: 3.063/7.067, observed IC $_{50}$: 3.716/7.342 μ M for 17f/17t as anti-HCT116, and estimated IC $_{50}$: 11.096/8.191, observed IC $_{50}$: 12.230/6.354 for 17b/17h as anti-PaCa2) are evidence for the goodness of these models which can be used for optimizing more potent analogs.

Conclusion

Spiroindolin-2-ones with phosphonate function 17a-t (20 analogs, 96-72% yield) were constructed in regioselective mode following microwave synthetic methodology for azomethine cycloaddition with the appropriate 3,5-bis(ylidene)-4-piperidone-1-phosphonate 14a-g. Different analytical techniques evidenced the structure, including single crystal X-ray studies of 17d. All the synthesized agents exhibited anti-HCT116 properties (MTT technique) with higher efficacies than the clinically approved drug, 5-fluorouracil. Compound 17h $(R=4-ClC_cH_a, R'=H)$ is the most promising agent synthesized with potency 6.6- and 3.1-folds that of the standard drugs, 5-fluorouracil and sunitinib, respectively. Additionally, promising anti-PaCa2 properties were noted for the synthesized agents 17a-t with higher potencies or close to that of sunitinib (clinically usable drug against pancreatic cancer). Compound 17f (R=4-FC₆H₄, R'=Cl) is the most promising anti-PaCa2 agent observed (3.2-fold that of sunitinib). It was observed that compound 17j ($R=4-ClC_6H_4$, R'=Cl) possesses anti-MCF7 potency close to that of 5-fluorouracil. Compound 17h (R=4-ClC₆H₄, R'=H; IC₅₀=4.149 μ M) is the most anti-A549 effective analog relative to doxorubicin. Some of the synthesized agents (17d, 17k, 17p, and 17s) revealed 3D-multilayer HCT116 cancer spheroid inhibitory properties. Needless to say that, the 3D-multicellular spheroid model is an important technique bridging the biological ability of a specific agent revealing a promising antiproliferation effect in the in vitro 2D-single layer culture with the in vivo animal model. Notable VEGFR-2 inhibitory properties were revealed by some of the synthesized analogs. The synthesized analogs also exhibited considerable COX-1/-2 inhibitory properties in addition to $TNF-\alpha$ relative to NSAIDs (ibuprofen and indomethacin, the clinically usable drugs). CAM testing supported the anti-VEGFR-2 observations and antiangiogenic properties. Internal and external validated QSAR models explored the functions necessary for the antitumor properties.

Experimental Chemical synthesis

Melting points were determined on a capillary point apparatus (Stuart SMP3) equipped with a digital thermometer. IR spectra (KBr) were recorded on a Shimadzu FT-IR 8400S spectrophotometer. Reactions were monitored using thin layer chromatography (TLC) on 0.2 mm silica gel F254 plates (Merck) utilizing various solvents for elution. The chemical structures of the synthesized compounds were characterized by nuclear magnetic resonance spectra (¹H-NMR, ¹³C-NMR) and determined on a Bruker NMR spectrometer (500 MHz, 125 MHz for ¹H and ¹³C, respectively). ¹³C-NMR spectra are fully decoupled. Chemical shifts were reported in parts per million (ppm) using the deuterated solvent peak or tetramethylsilane as an internal standard. The microwave oven used is a Milestone Italy (model: StartSynth, Reactor: Pack2B Basic Single Vessel Kit).

Synthesis of dispiro[indoline-3,2'-pyrrolidine-3',3''-piperidin]-1''-yl)phosphonates 17a-t (general procedure)

A mixture of equimolar amounts of the appropriate diethyl [3,5-di((*E*)-ylidene)-4-oxopiperidin-1-yl] phosphonates 14a-g (1.25 mmoL) and the corresponding isatins 15a-d with sarcosine 16 in ethanol (10 mL) was heated in the microwave reactor at 60 °C (60 Watt) for 90 min. (hold time). After the completion of the reaction (TLC), the reaction mixture was allowed to cool at room temperature, and the solvent was evaporated under reduced pressure. The separated solid upon triturating the residual material with methanol (5 mL) was collected and crystallized from a suitable solvent affording the corresponding 17a-t.

Diethyl (E)-(5''-benzylidene-1'-methyl-2,4''-dioxo-4'-phenyldispiro[indoline-3,2'-pyrrolidine-3',3''-piperidin]-1''-yl)phosphonate (17a)

Obtained from the reaction of 14a, 15a and 16, as pale yellow microcrystals from ethanol (92%), mp $181-182^{\circ}C^{43}$, and yield 92% (0.67 g).

Diethyl (E)-(5''-benzylidene-5-fluoro-1'-methyl-2,4''-dioxo-4'-phenyldispiro[indoline-3,2'-pyrrolidine-3',3''-piperidin]-1''-yl)phosphonate (17b)

Obtained from the reaction of 14a, 15b, and 16, as yellow microcrystals from methanol (80%), mp 212-214 °C and, yield 82% (0.62 g). IR: $v_{\rm max}/{\rm cm}^{-1}$ 3198, 1717, 1682, 1593, 1489, 1466, 1242, 1196, 1161, 1026. 1 H-NMR (DMSO- d_6) δ (ppm): 0.84 (t, J=6.0 Hz, 3H, CH $_3$), 0.99 (t, J=6.0 Hz, 3H, CH $_3$), 1.97 (s, 3H, NCH $_3$), 2.16 (d, J=13.4 Hz, 1H, upfield H of piperidinyl H $_2$ C-2′′), 3.31 (t, J=8.5 Hz, 1H, upfield H of pyrrolidinyl H $_2$ C-5′), 3.67–3.89 (m, 6H, downfield H of piperidinyl H $_2$ C-2′′+ downfield H of piperidinyl H $_2$ C-6′′+ 2 OCH $_2$), 4.65 (t, J=9.2 Hz, 1H, pyrrolidinyl HC-4′), 6.63–6.68 (m, 2H, arom. H), 6.98 (t, J=9.1 Hz, 1H, arom. H), 7.13 (d, J=7.4 Hz, 2H, arom. H), 7.26 (t, J=7.5 Hz, 1H, arom. H), 7.33–7.45 (m, 8H, 7 arom. H+olefinic CH), 10.55 (s, 1H, NH). 13 C-NMR (DMSO- d_6) δ (ppm): 15.51, 15.56, 15.75, 15.79 (CH $_3$), 33.9 (NCH $_3$), 45.4 (pyrrolidinyl HC-4′), 46.3 (piperidinyl H $_2$ C-6′′), 47.6 (piperidinyl H $_2$ C-2′′), 57.3 (pyrrolidinyl H $_2$ C-5′), 61.87, 61.91, 61.96, 62.27, 62.34 [spiro-C-3′ (C-3′′)+OCH $_2$], 75.4 [spiro-C-3 (C-2′)], 109.87, 109.93, 114.1, 114.3, 115.2, 115.4, 127.0, 127.2, 127.3, 128.3, 128.6, 129.3, 129.5, 129.8, 131.7, 131.8, 134.0, 137.95, 137.98, 139.9, 156.6, 158.5 (arom. C+olefinic C), 175.2, 197.2 (C=O). Anal. Calcd. for C $_3$ 3H $_3$ 5FN $_3$ O $_5$ P (603.63): C, 65.66; H, 5.84; N, 6.96. Found: C, 65.52; H, 5.80; N, 7.03.

Diethyl (E)-(5''-benzylidene-5-chloro-1'-methyl-2,4''-dioxo-4'-phenyldispiro[indoline-3,2'-pyrrolidine-3',3''-piperidin]-1''-yl)phosphonate (17c)

Obtained from the reaction of 14a, 15c and 16, as buff microcrystals from ethanol (94%), mp 220-221°C⁴³, and yield 94% (0.72 g).

Diethyl (*E*)-(5''-benzylidene-1',5-dimethyl-2,4''-dioxo-4'-phenyldispiro[indoline-3,2'-pyrrolidine-3',3''-piperidin]-1''-yl)phosphonate (17d)

Obtained from the reaction of 14a, 15d, and 16, as yellow microcrystals from methanol (80%), mp 210–212 °C, and yield 91% (0.68 g). IR: $v_{\rm max}/{\rm cm}^{-1}$ 3194, 1709, 1682, 1620, 1589, 1493, 1447, 1246, 1165, 1026. ¹H-NMR (DMSO- d_c) δ (ppm): 0.86 (t, J=8.8 Hz, 3H, CH₃), 0.98 (t, J=8.9 Hz, 3H, CH₃), 1.94 (s, 3H, NCH₃), 2.12 (br s, 1H, upfield H of piperidinyl H₂C-2''), 2.17 (s, 3H, ArCH₃), 3.27–3.34 (m, 2H, upfield H of pyrrolidinyl H₂C-5'+upfield H of upfield H of piperidinyl H₂C-6''+2 oxidesign oxide

Diethyl (*E*)-[5''-(4-fluorobenzylidene)-4'-(4-fluorophenyl)-1'-methyl-2,4''-dioxodispiro[indoline-3,2'-pyrrolidine-3',3''-piperidin]-1''-yl]phosphonate (17e)

Obtained from the reaction of 14b, 15a and 16, as pale yellow microcrystals from methanol, mp 193-194°C⁴³, and yield 95% (0.73 g).

Diethyl (E)-[5-chloro-5"-(4-fluorobenzylidene)-4'-(4-fluorophenyl)-1'-methyl-2,4"-dioxodispiro[indoline-3,2'-pyrrolidine-3',3"-piperidin]-1"-yl]phosphonate (17f)

Obtained from the reaction of 14b, 15c and 16, as pale yellow microcrystals from n-butanol, mp $234-235^{\circ}C^{43}$, and yield 92% (0.76 g).

Diethyl (E)-(5''-(4-fluorobenzylidene)-4'-(4-fluorophenyl)-1',5-dimethyl-2,4''-dioxodispiro[indoline-3,2'-pyrrolidine-3',3''-piperidin]-1''-yl)phosphonate (17g)

Obtained from the reaction of 14b, 15d, and 16, as pale yellow microcrystals from benzene, mp 216–217 °C, and yield 78% (0.62 g). IR: $v_{\rm max}/{\rm cm}^{-1}$ 3190, 1709, 1686, 1601, 1508, 1470, 1304, 1234, 1161, 1026. ¹H-NMR (DMSO- d_0) δ (ppm): 0.88 (t, J = 8.3 Hz, 3H, CH₃), 1.00 (t, J = 7.2 Hz, 3H, CH₃), 1.93 (s, 3H, NCH₃), 2.16 (s, 3H, ArCH₃), 2.19 (br s, 1H, upfield H of piperidinyl H₂C-2''), 3.30–3.32 (m, 2H, upfield H of pyrrolidinyl H₂C-5' + upfield H of upfield H of piperidinyl H₂C-6''), 3.49–3.57 (m, 1H, downfield H of pyrrolidinyl H₂C-5'), 3.66–3.80 (m, 6H, downfield H of piperidinyl H₂C-2'' + downfield H of piperidinyl H₂C-6'' + 2 OCH₂), 4.67 (t, J = 9.2 Hz, 1H, pyrrolidinyl HC-4'), 6.58 (d, J = 7.9 Hz, 1H, arom. H), 6.68 (s, 1H, arom. H), 6.93 (d, J = 7.9 Hz, 1H, arom. H), 7.14–7.18 (m, 4H, arom. H), 7.25 (t, J = 9.0 Hz, 2H, arom. H), 7.43–7.51 (m, 3H, arom. H + olefinic CH), 10.42 (s, 1H, NH). ¹³C-NMR (DMSO- d_6) δ (ppm): 15.58, 15.63, 15.75, 15.80 (CH₃), 20.6 (ArCH₃), 33.8 (NCH₃), 45.3 (pyrrolidinyl HC-4'), 45.4 (piperidinyl H₂C-6''), 47.4 (piperidinyl H₂C-2''), 57.6 (pyrrolidinyl H₂C-5'), 61.6, 61.7, 61.84, 61.86, 61.89, 61.91 [spiro-C-3' (C-3'') + OCH₃], 75.3 [spiro-C-3 (C-2')], 108.9, 114.8, 115.0, 115.6, 115.8, 125.3, 127.4, 129.1, 129.5, 130.67, 130.70, 131.65, 131.73, 131.79, 131.9, 132.0, 134.38, 134.41, 136.2, 141.2, 160.2, 161.2, 162.1, 163.2 (arom. C + olefinic C), 175.2, 196.9 (C = O). Anal. Calcd. for C₃₄H₃₆F₂N₃O₅P (635.65): C, 64.25; H, 5.71; N, 6.61. Found: C, 64.46; H, 5.85; N, 6.80.

Diethyl (*E*)-[5''-(4-chlorobenzylidene)-4'-(4-chlorophenyl)-1'-methyl-2,4''-dioxodispiro[indoline-3,2'-pyrrolidine-3',3''-piperidin]-1''-yl]phosphonate (17h)

Obtained from the reaction of 14c, 15a and 16, as pale yellow microcrystals from benzene – light petroleum as 1.2 v/v, mp $143-145^{\circ}\text{C}^{43}$, and yield 91% (0.74 g).

Diethyl (E)-(5''-(4-chlorobenzylidene)-4'-(4-chlorophenyl)-5-fluoro-1'-methyl-2,4''-dioxodispiro[indoline-3,2'-pyrrolidine-3',3''-piperidin]-1''-yl)phosphonate (17i)

Obtained from the reaction of 14c, 15b, and 16, as yellow microcrystals from methanol, mp 208–210 °C, and yield 93% (0.78 g). IR: $\nu_{\rm max}/{\rm cm}^{-1}$ 3190, 1709, 1678, 1605, 1489, 1466, 1304, 1238, 1192, 1026. $^{\rm 1}{\rm H}$ -NMR (DMSO- d_6) & (ppm): 0.86 (t, J = 8.2 Hz, 3H, CH₃), 1.02 (br s, 3H, CH₃), 1.95 (s, 3H, NCH₃), 2.23 (d, J = 13.5 Hz, 1H, upfield H of piperidinyl H₂C-2′′), 3.33 (t, J = 8.7 Hz, 1H, upfield H of pyrrolidinyl H₂C-5′), 3.43 (d, J = 15.5, Hz, 1H, upfield H of upfield H of piperidinyl H₂C-6′′), 3.49–3.56 (m, 1H, downfield H of pyrrolidinyl H₂C-5′), 3.69–3.83 (m, 6H, downfield H of piperidinyl H₂C-2′′ + downfield H of piperidinyl H₂C-6′′ + 2 OCH₂), 4.61 (t, J = 9.4 Hz, 1H, pyrrolidinyl HC-4′), 6.61–6.68 (m, 2H, arom. H), 6.98 (t, J = 8.7 Hz, 1H, arom. H), 7.16 (d, J = 7.8 Hz, 2H, arom. H), 7.38–7.49 (m, 7H, 6 arom. H + olefinic CH), 10.59 (s, 1H, NH). $^{\rm 13}$ C-NMR (DMSO- d_6) & (ppm): 15.55, 15.60, 15.76, 15.81 (CH₃), 33.8 (NCH₃), 45.5 (pyrrolidinyl HC-4′), 45.7 (piperidinyl H₂C-6′′), 47.5 (piperidinyl H₂C-2′′), 57.5 (pyrrolidinyl H₂C-5′), 61.95, 61.99, 62.0, 62.1, 62.2 [spiro-C-3′ (C-3′′) + OCH₂], 75.5 [spiro-C-3 (C-2′′)], 110.0, 110.1, 114.1, 114.3, 115.3, 115.5, 126.98, 127.04, 128.2, 128.7, 128.8, 131.3, 131.7, 131.8, 132.1, 132.2, 132.3, 132.8, 134.1, 136.5, 137.0, 139.9, 156.6, 158.5 (arom. C+olefinic C), 175.2, 196.9 (C = O). Anal. Calcd. for $C_{33}H_{33}Cl_2FN_3O_5P$ (672.52): C, 58.94; H, 4.95; N, 6.25. Found: C, 59.06; H, 5.11; N, 6.34.

Diethyl (*E*)-[5-chloro-5"-(4-chlorobenzylidene)-4'-(4-chlorophenyl)-1'-methyl-2,4"-dioxodispiro[indoline-3,2'-pyrrolidine-3',3"-piperidin]-1"-yl]phosphonate (17j)
Obtained from the reaction of 14c, 15c and 16, as pale yellow microcrystals from methanol, mp 229-230°C⁴³, and yield 89% (0.76 g).

Diethyl (E)-(5''-(4-chlorobenzylidene)-4'-(4-chlorophenyl)-1',5-dimethyl-2,4''-dioxodispiro[indoline-3,2'-pyrrolidine-3',3''-piperidin]-1''-yl)phosphonate (17k)

Obtained from the reaction of 14c, 15d, and 16, as yellow microcrystals from methanol, mp 208-209 °C, and yield 95% (0.79 g). IR: $v_{\rm max}/{\rm cm}^{-1}$ 3186, 1705, 1686, 1605, 1493, 1470, 1304, 1238, 1026. ¹H-NMR (DMSO- d_e) δ (ppm): 0.87 (t, J=7.2 Hz, 3H, CH₃), 1.00 (t, J=8.6 Hz, 3H, CH₃), 1.92 (s, 3H, NCH₃), 2.16 (s, 3H, ArCH₃), 2.21 (br s, 1H, upfield H of piperidinyl H₂C-2′′), 3.30–3.33 (m, 2H, upfield H of pyrrolidinyl H₂C-5′ + upfield H of upfield H of piperidinyl H₂C-6′′), 3.49–3.54 (m, 1H, downfield H of pyrrolidinyl H₂C-5′), 3.65–3.76 (m, 6H, downfield H of piperidinyl H₂C-2′′ + downfield H of piperidinyl H₂C-6′′ + 2 OCH₂), 4.64 (t, J=10.0 Hz, 1H, pyrrolidinyl HC-4′), 6.57 (d, J=5.0 Hz, 1H, arom. H), 6.67 (s, 1H, arom. H), 6.93 (d, J=7.8 Hz, 1H, arom. H), 7.14 (d, J=8.3 Hz, 2H, arom. H), 7.39–7.49 (m, 7H, 6 arom. H + olefinic CH), 10.47 (s, 1H, NH). ¹³C-NMR (DMSO- d_e) δ (ppm): 15.66, 15.71, 15.8, 15.9 (CH₃), 20.7 (ArCH₃), 33.9 (NCH₃), 45.4 (pyrrolidinyl HC-4′), 45.5 (piperidinyl H₂C-6′′), 47.5 (piperidinyl H₂C-2′′), 57.5 (pyrrolidinyl H₂C-5′), 61.7, 61.8, 61.94, 61.96, 62.00 [spiro-C-3′ (C-3′′) + OCH₂], 75.3 [spiro-C-3 (C-2′′)], 109.0, 125.2, 127.5, 128.2, 128.8, 129.2, 129.6, 131.4, 131.6, 131.9, 132.4, 132.5, 133.0, 134.0, 136.1, 137.3, 141.2 (arom. C + olefinic C), 175.2, 196.8 (C = O). Anal. Calcd. for $C_{34}H_{36}$ Cl₂N₃O₅P (668.55): C, 61.08; H, 5.43; N, 6.29. Found: C, 60.92; H, 5.35; N, 6.46.

Diethyl (*E*)-[5''-(4-bromobenzylidene)-4'-(4-bromophenyl)-1'-methyl-2,4''-dioxodispiro[indoline-3,2'-pyrrolidine-3',3''-piperidin]-1''-yl]phosphonate (17l) Obtained from the reaction of 14d, 15a and 16, as pale yellow microcrystals from methanol, mp 137-139°C⁴³, and yield 85% (0.79 g).

Diethyl (E)-[1'-methyl-5''-(4-methylbenzylidene)-2,4''-dioxo-4'-(p-tolyl)dispiro[indoline-3,2'-pyrrolidine-3',3''-piperidin]-1''-yl]phosphonate (17m)

Obtained from the reaction of 14e, 15a and 16, as pale yellow microcrystals from methanol, mp 226-227°C⁴³, and yield 96% (0.73 g).

Diethyl (E)-(5-fluoro-1'-methyl-5''-(4-methylbenzylidene)-2,4''-dioxo-4'-(p-tolyl) dispiro[indoline-3,2'-pyrrolidine-3',3''-piperidin]-1''-yl)phosphonate (17n)

Obtained from the reaction of 14e, 15b, and 16, as yellow microcrystals from methanol, mp 179-181 °C, and yield 93% (0.73 g). IR: $v_{\rm max}/{\rm cm}^{-1}$ 3194, 1713, 1674, 1593, 1512, 1489, 1470, 1300, 1234, 1196, 1026. ¹H-NMR (DMSO- d_c) δ (ppm): 0.87 (br s, 3H, CH₃), 1.01 (t, J = 8.3 Hz, 3H, CH₃), 1.95 (s, 3H, NCH₃), 2.16 (d, J = 13.3 Hz, 1H, upfield H of piperidinyl H₂C-2′′), 2.28 (s, 3H, ArCH₃), 2.30 (s, 3H, ArCH₃), 3.44 (d, J = 15.2 Hz, 1H, upfield H of upfield H of piperidinyl H₂C-5′′), 3.50–3.55 (m, 1H, upfield H of pyrrolidinyl H₂C-5′), 3.66–3.86 (m, 7H, downfield H of pyrrolidinyl H₂C-5′+ downfield H of piperidinyl H₂C-2′′+ downfield H of piperidinyl H₂C-6′′+2 OCH₂), 4.60 (t, J = 9.3 Hz, 1H, pyrrolidinyl HC-4′), 6.61–6.66 (m, 2H, arom. H), 6.96 (t, J = 9.3 Hz, 1H, arom. H), 7.04 (d, J = 7.7 Hz, 2H, arom. H), 7.14 (d, J = 7.6 Hz, 2H, arom. H), 7.22 (d, J = 7.3 Hz, 2H, arom. H), 7.31 (d, J = 7.5 Hz, 2H, arom. H), 7.39 (s, 1H, olefinic CH), 10.53 (s, 1H, NH). ¹³C-NMR (DMSO- d_c) δ (ppm): 15.6, 15.78, 15.83 (CH₃), 20.6, 20.9 (ArCH₃), 33.9 (NCH₃), 45.5 (pyrrolidinyl HC-4′), 45.9 (piperidinyl H₂C-6′′), 47.5 (piperidinyl H₂C-2′′), 57.4 (pyrrolidinyl H₂C-5′), 62.0, 62.2 [spiro-C-3′ (C-3′′) + OCH₂], 75.4 [spiro-C-3 (C-2′)], 109.9, 128.9, 129.3, 129.7, 129.8, 130.5, 130.8, 131.2, 134.9, 136.1, 138.0, 139.4, 139.9 (arom. C + olefinic C), 175.2, 197.2 (C=O). Anal. Calcd. for $C_{35}H_{39}FN_3O_5P$ (631.69): C, 66.55; H, 6.22; N, 6.65. Found: C, 66.77; H, 6.31; N, 6.76.

Diethyl (E)-[5-chloro-1'-methyl-5''-(4-methylbenzylidene)-2,4''-dioxo-4'-(p-tolyl) dispiro[indoline-3,2'-pyrrolidine-3',3''-piperidin]-1''-yl]phosphonate (17o)

Obtained from the reaction of 14e, 15c and 16, as pale yellow microcrystals from ethyl acetate, mp 227-228°C⁴³, and yield 93% (0.75 g).

Diethyl (E)-[5''-(4-methoxybenzylidene)-4'-(4-methoxyphenyl)-1'-methyl-2,4''-dioxodispiro[indoline-3,2'-pyrrolidine-3',3''-piperidin]-1''-yl]phosphonate (17p)

Obtained from the reaction of 14f., 15a and 16, as pale yellow microcrystals from methanol, mp 196-198°C⁴³, and yield 88% (0.75 g).

Diethyl (*E*)-[1'-methyl-2,4''-dioxo-4'-(thiophen-2-yl)-5''-(thiophen-2-ylmethylene) dispiro[indoline-3,2'-pyrrolidine-3',3''-piperidin]-1''-yl]phosphonate (17q)

Obtained from the reaction of 14g, 15a and 16, as pale yellow microcrystals from methanol, mp 206-208°C⁴³, and yield 84% (0.62 g).

Diethyl (E)-(5-fluoro-1'-methyl-2,4"-dioxo-4'-(thiophen-2-yl)-5"-(thiophen-2-ylmethylene) dispiro[indoline-3,2'-pyrrolidine-3',3"-piperidin]-1"-yl)phosphonate (17r)

Obtained from the reaction of 14e, 15b, and 16, as yellow microcrystals from methanol (80%), mp 216–218 °C, and yield 77% (0.59 g). IR: $v_{\rm max}/{\rm cm}^{-1}$ 3194, 1713, 1674, 1574, 1489, 1462, 1300, 1246, 1196, 1026. ¹H-NMR (DMSO- $d_{\rm o}$) δ (ppm): 1.22 (t, J=7.1 Hz, 3H, CH $_{\rm o}$), 1.25 (t, J=7.3 Hz, 3H, CH $_{\rm o}$), 2.09 (s, 3H, NCH $_{\rm o}$), 2.58 (d, J=13.5 Hz, 1H, upfield H of piperidinyl H $_{\rm o}$ C-2′′), 3.78–4.13 (m, 7H, downfield H of pyrrolidinyl H $_{\rm o}$ C-5′ + downfield H of piperidinyl H $_{\rm o}$ C-5′ + downfield H of piperidinyl H $_{\rm o}$ C-2′′ + downfield H of piperidinyl H $_{\rm o}$ C-6′′ + 2 OCH $_{\rm o}$), 5.00 (t, J=9.2 Hz, 1H, pyrrolidinyl HC-4′), 6.70 (d, J=8.6 Hz, 1H, arom. H), 6.81–6.83 (m, 1H, arom. H), 7.08 (t, J=10.2 Hz, 1H, arom. H), 7.16 (br s, 1H, arom. H), 7.26 (br s, 1H, arom. H), 7.39 (br s, 1H, arom. H), 7.55 (br s, 1H, arom. H), 7.70–8.08 (m, 3H, 2 arom. H+olefinic CH), 10.70 (s, 1H, NH). 13 C-NMR (DMSO- $d_{\rm o}$) δ (ppm): 15.85, 15.90, 15.94 (CH $_{\rm o}$), 33.7 (NCH $_{\rm o}$), 40.9 (pyrrolidinyl HC-4′), 45.6 (piperidinyl H $_{\rm o}$ C-6′′), 46.0 (piperidinyl H $_{\rm o}$ C-2′′), 58.4 (pyrrolidinyl H $_{\rm o}$ C-5′), 61.4, 61.5, 61.96, 62.01, 62.06, 62.10 [spiro-C-3′ (C-3′′) + OCH $_{\rm o}$], 75.3 [spiro-C-3 (C-2′)], 109.89, 109.95, 113.7, 113.9, 115.2, 115.4, 125.0, 126.7, 126.9, 127.0, 127.2, 128.5, 130.4, 133.2, 135.2, 135.3, 137.0, 140.0, 140.7, 156.4, 158.3 (arom. C+olefinic C), 174.9, 195.6 (C=O). Anal. Calcd. for $C_{\rm o}$ H $_{\rm o}$ H $_{\rm o}$ FS $_{\rm o}$ C (615.68): C, 56.58; H, 5.08; N, 6.83. Found: C, 56.44; H, 5.19; N, 6.67.

Diethyl (E)-[5-chloro-1'-methyl-2,4''-dioxo-4'-(thiophen-2-yl)-5''-(thiophen-2-ylmethylene) dispiro[indoline-3,2'-pyrrolidine-3',3''-piperidin]-1''-yl]phosphonate (17s)

Obtained from the reaction of 14g, 15c and 16, as pale yellow microcrystals from methanol, mp 223-225°C⁴³, and yield 80% (0.63 g).

Diethyl (E)-(1',5-dimethyl-2,4''-dioxo-4'-(thiophen-2-yl)-5''-(thiophen-2-ylmethylene) dispiro[indoline-3,2'-pyrrolidine-3',3''-piperidin]-1''-yl)phosphonate (17t)

Obtained from the reaction of 14g, 15d, and 16, as yellow microcrystals from methanol, mp 202-204 °C, and yield 72% (0.55 g). IR: $v_{\text{max}}/\text{cm}^{-1}$ 3090, 1709, 1670, 1585, 1489, 1466, 1300, 1234, 1030. ¹H-NMR (DMSO- d_o) δ (ppm): 1.05–1.10 (m, 6H, 2 CH₃), 1.92 (s, 3H, NCH₃), 2.00 (s, 3H, ArCH₃), 2.40 (d, J=13.1 Hz, 1H, upfield H of piperidinyl H₂C-2′′), 3.36 (d, J=9.5 Hz, 2H, upfield H of pyrrolidinyl H₂C-5′ + upfield H of upfield H of piperidinyl H₂C-6′′), 3.65–3.93 (m, 7H, downfield H of pyrrolidinyl H₂C-5′ + downfield H of piperidinyl H₂C-2′′ + downfield H of piperidinyl H₂C-6′′ + 2 OCH₂), 4.90 (t, J=8.1 Hz, 1H, pyrrolidinyl HC-4′), 6.54 (br s, 1H, arom. H), 6.61 (br s, 1H, arom. H), 6.86 (br s, 1H, arom. H), 7.01 (br s, 1H, arom. H), 7.11 (br s, 1H, arom. H), 7.23 (br s, 1H, arom. H), 7.40 (br s, 1H, arom. H), 7.51–7.89 (m, 3H, 2 arom. H + olefinic CH), 10.40 (s,

1H, NH). $^{13}\text{C-NMR}$ (DMSO- d_6) δ (ppm): 15.9 (CH $_3$), 20.5 (ArCH $_3$), 33.8 (NCH $_3$), 40.5 (pyrrolidinyl HC-4′), 45.5 (piperidinyl H $_2\text{C-6''}$), 46.1 (piperidinyl H $_2\text{C-2''}$), 58.4 (pyrrolidinyl H $_2\text{C-5'}$), 61.1, 62.0 [spiro-C-3′ (C-3′′)+OCH $_2$], 75.1 [spiro-C-3 (C-2′)], 108.8, 124.92, 124.98, 127.0, 127.2, 127.4, 128.4, 129.0, 129.3, 129.9, 132.9, 134.7, 137.2, 141.0, 141.3 (arom. C+olefinic C), 174.9, 195.5 (C=O). Anal. Calcd. for $\text{C}_{30}\text{H}_{34}\text{N}_3\text{O}_5\text{PS}_2$ (611.71): C, 58.91; H, 5.60; N, 6.87. Found: C, 58.74; H, 5.48; N, 6.73.

Biological, biochemical and computational studies

The biological, biochemical and computational studies were mentioned in the supplementary file. The cell lines used in the current study were kindly gifted by Prof. Stig Linder, Karolinska Institute, Stockholm, Sweden, originally purchased from ATCC.

Data availability

All data generated or analyzed during this study are included in this published article and its supplementary material files. Crystallographic data for the structure reported in this paper **17d** has been deposited at the Cambridge Crystallographic Data Centre (CCDC) in the CSD under reference CCDC 2467603. These data can be obtained free of charge from the CCDC via https://www.ccdc.cam.ac.uk/structures/.

Received: 7 July 2025; Accepted: 16 September 2025

Published online: 07 October 2025

References

- Zhang, R., Yao, Y., Gao, H. & Hu, X. Mechanisms of angiogenesis in tumour. Front. Oncol. 14, 1359069. https://doi.org/10.3389/fonc.2024.1359069 (2024).
- Carmeliet, P. & Jain, R. K. Molecular mechanisms and clinical applications of angiogenesis. Nature 473, 298–307. https://doi.org/10.1038/nature10144 (2011).
- 3. Liu, Z.-L., Chen, H.-H., Zheng, L.-L., Sun, L.-P. & Shi, L. Angiogenic signaling pathways and anti-angiogenic therapy for cancer. Signal Transduct. Target. Ther. 8, 198. https://doi.org/10.1038/s41392-023-01460-1 (2023).
- 4. Nakamura, H. et al. Synthesis and biological evaluation of benzamides and benzamidines as selective inhibitors of VEGFR tyrosine kinases. *Bioorg. Med. Chem. Lett.* **16**, 5127–5131. https://doi.org/10.1016/j.bmcl.2006.07.075 (2006).
- 5. Sorafenib, uses, interactions, mechanism of action, (accessed 29 June 2025); https://go.drugbank.com/drugs/DB00398
- 6. Nexavar (sorafenib) FDA approval history, (accessed 29 June 2025); https://www.drugs.com/history/nexavar.html
- 7. Regorafenib, uses, interactions, mechanism of action, (accessed 29 June 2025); https://go.drugbank.com/drugs/DB08896
- 8. Stivarga (Regorafenib) FDA Approval History, (accessed 29 June 2025); https://www.drugs.com/history/stivarga.html
- 9. Lenvatinib mesylate, (accessed 29 June 2025); https://go.drugbank.com/salts/DBSALT001109
- 10. Lenvima (lenvatinib) FDA approval history, (accessed 29 June 2025); https://www.drugs.com/history/lenvima.html
- 11. Cabozantinib, uses, interactions, mechanism of action, (accessed 29 June 2025); https://go.drugbank.com/drugs/DB08875
- 12. Cabometyx (cabozantinib) FDA Approval History, (accessed 29 June 2025); https://www.drugs.com/history/cabometyx.html
- 13. Vandetanib, uses, interactions, mechanism of action, (accessed 29 June 2025); https://go.drugbank.com/drugs/DB05294
- $14. \ \ Caprelsa\ (Van detanib)\ FDA\ approval\ history, (accessed\ 29\ June\ 2025);\ https://www.drugs.com/history/caprelsa.html$
- 15. Pazopanib, uses, interactions, mechanism of action, (accessed 29 June 2025); https://go.drugbank.com/drugs/DB06589
 16. Votrient (Pazopanib) FDA Approval History, (accessed 29 June 2025); https://www.drugs.com/history/votrient.html
- 17. Axitinib, uses, interactions, mechanism of action, (accessed 29 June 2025); https://go.drugbank.com/drugs/DB06626
- 18. Inlyta (Axitinib) FDA approval history, (accessed 29 June 2025); https://www.drugs.com/history/inlyta.html
- 19. Sunitinib, uses, interactions, mechanism of action, (accessed 29 June 2025); https://go.drugbank.com/drugs/DB01268
- 20. Sutent (sunitinib malate) FDA approval history, (accessed 29 June 2025); https://www.drugs.com/history/sutent.html
- 21. Aboshouk, D. R. et al. Design and synthesis of antiproliferative 2-oxoindolin-3-ylidenes incorporating urea function with potential VEGFR-2 inhibitory properties. *Sci. Rep.* 15, 618. https://doi.org/10.1038/s41598-024-82005-6 (2025).
- Thakur, A. et al. Recent advances and future directions on small molecule VEGFR inhibitors in oncological conditions. Eur. J. Med. Chem. 272, 116472. https://doi.org/10.1016/j.ejmech.2024.116472 (2024).
- 23. Girgis, A. S. et al. 3-Alkenyl-2-oxindoles: Synthesis, antiproliferative and antiviral properties against SARS-CoV-2. *Bioorg. Chem.* 114, 105131. https://doi.org/10.1016/j.bioorg.2021.105131 (2021).
- 24. Abuzenadah, A. M. et al. Elucidating antiangiogenic potential of Rauwolfia serpentina: VEGFR-2 targeting-based molecular docking study. Evid. Based Complement. Alternat. Med. https://doi.org/10.1155/2022/6224666 (2022).
- Farghaly, T. A., Al-Hasani, W. A. & Abdulwahab, H. G. An updated patent review of VEGFR-2 inhibitors (2017-present). Expert Opin. Ther. Pat. 31, 989–1007. https://doi.org/10.1080/13543776.2021.1935872 (2021).
- Seliem, I. A. et al. Development of isatin-based Schiff bases targeting VEGFR-2 inhibition: Synthesis, characterization, antiproliferative properties, and QSAR studies. ChemMedChem 17, e202200164. https://doi.org/10.1002/cmdc.202200164 (2022).
- Aboshouk, D. R., Youssef, M. A., Bekheit, M. S., Hamed, A. R. & Girgis, A. S. Antineoplastic indole-containing compounds with potential VEGFR inhibitory properties. RSC Adv. 14, 5690–5728. https://doi.org/10.1039/D3RA08962B (2024).
- 28. Hassan, S. M. et al. Indole compounds in oncology: therapeutic potential and mechanistic insights. *Pharmaceuticals* 17, 922. https://doi.org/10.3390/ph17070922 (2024).
- 29. Adefovir: Uses, interactions, mechanism of action, (accessed 29 June 2025); https://go.drugbank.com/drugs/DB13868
- 30. Cidofovir: Uses, interactions, mechanism of action, (accessed 29 June 2025); https://go.drugbank.com/drugs/DB00369
- 31. Zoledronic acid, (accessed 29 June 2025); https://go.drugbank.com/drugs/DB00399

i.org/10.1016/j.addr.2007.05.013 (2007).

- 32. Adefovir dipivoxil: Uses, interactions, mechanism of action, (accessed June 29 2025); https://go.drugbank.com/drugs/DB00718
- 33. Tenofovir disoproxil: Uses, interactions, mechanism of action, (accessed 29 June 2025); https://go.drugbank.com/drugs/DB00300
 34. Stella, V. J. & Nti-Addae, K. W. Prodrug strategies to overcome poor water solubility. Adv. Drug Deliv. Rev. 59, 677–694. https://do
- 35. Sauer, R. et al. Water-soluble phosphate prodrugs of 1-propargyl-8-styrylxanthine derivatives, A_{2A}-selective adenosine receptor antagonists. *J. Med. Chem.* 43, 440–448. https://doi.org/10.1021/jm9911480 (2000).
- 36. Lockbaum, G. J. et al. HIV-1 protease inhibitors with a P1 phosphonate modification maintain potency against drug-resistant variants by increased interactions with flap residues. *Eur. J. Med. Chem.* 257, 115501. https://doi.org/10.1016/j.ejmech.2023.115501 (2023).
- Girgis, A. S. et al. The therapeutic potential of spirooxindoles in cancer: A focus on p53–MDM2 modulation. *Pharmaceuticals* 18, 274. https://doi.org/10.3390/ph18020274 (2025).

- 38. Fawazy, N. G. et al. Development of spiro-3-indolin-2-one containing compounds of antiproliferative and anti-SARS-CoV-2 properties. Sci. Rep. 12, 13880. https://doi.org/10.1038/s41598-022-17883-9 (2022).
- 39. Panda, S. S., Girgis, A. S., Aziz, M. N. & Bekheit, M. S. Spirooxindole: A versatile biologically active heterocyclic scaffold. *Molecules* 28, 618. https://doi.org/10.3390/molecules28020618 (2023).
- Girgis, A. S. et al. Synthesis, and QSAR analysis of anti-oncological active spiro-alkaloids. Org. Biomol. Chem. 13, 1741–1753. https://doi.org/10.1039/C4OB02149E (2015).
- 41. Panda, S. S. et al. Rational design, synthesis and molecular modeling studies of novel anti-oncological alkaloids against melanoma. *Org. Biomol. Chem.* 13, 6619–6633. https://doi.org/10.1039/C5OB00410A (2015).
- 42. Choudhury, C., Kumar, V. & Kumar, R. smProdrugs: A repository of small molecule prodrugs. Eur. J. Med. Chem. 249, 115153. https://doi.org/10.1016/j.ejmech.2023.115153 (2023).
- Bekheit, M. S. et al. Spiroindole-containing compounds bearing phosphonate group of potential M^{pro}-SARS-CoV-2 inhibitory properties. Eur. J. Med. Chem. 258, 115563. https://doi.org/10.1016/j.ejmech.2023.115563 (2023).
- Díaz-Carballo, D. et al. Therapeutic potential of antiviral drugs targeting chemorefractory colorectal adenocarcinoma cells overexpressing endogenous retroviral elements. J. Exp. Clin. Cancer Res. 34, 81. https://doi.org/10.1186/s13046-015-0199-5 (2015).
- 45. Fawzy, N. G. et al. Novel curcumin inspired antineoplastic 1-sulfonyl-4-piperidones: Design, synthesis and molecular modeling studies. Anti-Cancer Agents Med. Chem. 19, 1069–1078. https://doi.org/10.2174/1871520619666190408131639 (2019).
- 46. Fluorouracil injection Uses, Side Effects & Warnings, (accessed June 29 2025); https://www.drugs.com/mtm/fluorouracil-injection.html
- 47. Fluorouracil topical Uses, Side Effects & Warnings, (accessed 29 June 2025); https://www.drugs.com/mtm/fluorouracil-topical.ht
- 48. Doxorubicin: Uses, Interactions, Mechanism of Action, (accessed 29 June 2025); https://go.drugbank.com/drugs/DB00997
- 49. Roy, A., Raza, M. A. & Ghosh, V. Ajazuddin, diagnostic innovations and therapeutic potential of nanoparticulate delivery for colon cancer. *Nano-Struct. Nano-Obj.* 41, 101426. https://doi.org/10.1016/j.nanoso.2024.101426 (2025).
- 50. Gan, A. W., Kang, X., Goh, S. S., Wong, S. H. & Loo, S. C. J. Recent advances in the encapsulation of probiotics as functional foods for colorectal cancer prevention. *J. Funct. Foods* **128**, 106804. https://doi.org/10.1016/j.jff.2025.106804 (2025).
- Zhang, J. et al. Metabolic reprogramming of drug resistance in pancreatic cancer: Mechanisms and effects. Mol Aspects Med. 103, 101368. https://doi.org/10.1016/j.mam.2025.101368 (2025).
- 52. Sharma, R., Komal, K., Kuma, S., Ghosh, R. & Kumar, M. A comprehensive review on revolutionizing pancreatic cancer treatment: Liposomal innovations. *J. Drug Deli. Sci. Technol.* 110, 107032. https://doi.org/10.1016/j.jddst.2025.107032 (2025).
- Elposoniai initovations. J. Drug Dett. Sct. Technol. 110, 107032. https://doi.org/10.1016/j.jddst.2023.107032 (2023).

 53. Zaki-Dizaji, M., Taheri, Z., Heiat, M. & Hushmand, K. Tumor-educated platelet, a potential liquid biopsy biosource in pancreatic
- cancer: A review. *Pathol. Res. Pract.* **270**, 155986. https://doi.org/10.1016/j.prp.2025.155986 (2025).

 54. Gautam, S. et al. Understanding drug resistance in breast cancer: Mechanisms and emerging therapeutic strategies. *Medicine in*
- Drug Discovery 26, 100210. https://doi.org/10.1016/j.medidd.2025.100210 (2025).

 55. Zhou, Z. et al. LAT1 transporter as a target for breast cancer diagnosis and therapy. Eur. J. Med. Chem. 283, 117064. https://doi.org/
- g/10.1016/j.ejmech.2024.117064 (2025).
 56. Selvamuthukumar, K. et al. Recent advances in breath-based volatile compounds analysis by various analytical techniques for
- screening of lung cancer disease. *Microchem. J.* **214**, 114003. https://doi.org/10.1016/j.microc.2025.114003 (2025).

 57. Feng, Y. et al. Targeting CAFs and extracellular matrix (ECM) in lung cancer: Potential of adjuvants and nanoparticles. *Bioorg*.
- *Chem.* **162**, 108586. https://doi.org/10.1016/j.bioorg.2025.108586 (2025).

 58. Davoodi, F. et al. Theranostic applications of graphene-based materials in lung cancer: A review. *FlatChem* **51**, 100871. https://doi
- .org/10.1016/j.flatc.2025.100871 (2025).
 59. Lama, R. et al. Development, validation and pilot screening of an in vitro multi-cellular three-dimensional cancer spheroid assay
- for anti-cancer drug testing. *Bioorg. Med. Chem.* 21, 922–931. https://doi.org/10.1016/j.bmc.2012.12.007 (2013).

 60. Mendes, V. I. S., Bartholomeusz, G. A., Ayres, M., Gandhi, V. & Salvador, J. A. R. Synthesis and cytotoxic activity of novel A-ring cleaved ursolic acid derivatives in human non-small cell lung cancer cells. *Eur. J. Med. Chem.* 123, 317–331. https://doi.org/10.101
- 6/j.ejmech.2016.07.045 (2016).
 61. Ivascu, A. & Kubbies, M. Rapid generation of single-tumor spheroids for high-throughput cell function and toxicity analysis. *J. Biomol. Screen.* 11, 922–932. https://doi.org/10.1177/1087057106292763 (2006).
- Friedrich, J. et al. A reliable tool to determine cell viability in complex 3-D culture: The acid phosphatase assay. J. Biomol. Screen. 12, 925–937. https://doi.org/10.1177/1087057107306839 (2007).
- 63. Human VEGF R2 ELISA Kit, ELH-VEGFR2, RayBiotech, Peachtree Corners, GA, www.RayBiotech.com.
- 64. Brown, L. D. et al. Novel isatin conjugates endowed with analgesic and anti-inflammatory properties: Design, synthesis and biological evaluation. Future Med. Chem. 17, 59–73. https://doi.org/10.1080/17568919.2024.2437981 (2025).
- 65. Wang, G. et al. Two new neolignans and an indole alkaloid from the stems of *Nauclea officinalis* and their biological activities. *Fitoterapia* 160, 105228. https://doi.org/10.1016/j.fitote.2022.105228 (2022).
- 66. Kumar, R. S. et al. Functionalized spirooxindole-indolizine hybrids: Stereoselective green synthesis and evaluation of anti-inflammatory effect involving TNF-α and nitrite inhibition. Eur. J. Med. Chem. 152, 417–423. https://doi.org/10.1016/j.ejmech.20 18.04.060 (2018).
- 67. Coussens, L. M. & Werb, Z. Inflammation and cancer. Nature 420, 860-867. https://doi.org/10.1038/nature01322 (2002).
- 68. Zhao, H. et al. Inflammation and tumor progression: Signaling pathways and targeted intervention. Signal Transduct. Target. Ther. 6, 263. https://doi.org/10.1038/s41392-021-00658-5 (2021).
- 69. Mercogliano, M. F., Bruni, S., Mauro, F., Elizalde, P. V. & Schillaci, R. Harnessing tumor necrosis factor alpha to achieve effective cancer immunotherapy. *Cancers* 13, 564. https://doi.org/10.3390/cancers13030564 (2021).
- Hirano, T. IL-6 in inflammation, autoimmunity and cancer. Int. Immunol. 33, 127–148. https://doi.org/10.1093/intimm/dxaa078 (2021).
- 71. Rašková, M. et al. The role of IL-6 in cancer cell invasiveness and metastasis-overview and therapeutic opportunities. *Cells* 11, 3698. https://doi.org/10.3390/cells11223698 (2022).
- 72. Bell, C. R. et al. Chemotherapy-induced COX-2 upregulation by cancer cells defines their inflammatory properties and limits the efficacy of chemoimmunotherapy combinations. *Nat. Commun.* 13, 2063. https://doi.org/10.1038/s41467-022-29606-9 (2022).
- 73. Pu, D. et al. Cyclooxygenase-2 inhibitor: A potential combination strategy with immunotherapy in cancer. Front. Oncol. 11, 637504. https://doi.org/10.3389/fonc.2021.637504 (2021).
- 74. COX-1 inhibitor screening kit, fluorometric (catalog # K548-100), BioVision incorporated USA, www.biovision.com
- 75. COX-2 inhibitor screening kit, fluorometric (catalog # K548–100), BioVision incorporated USA, www.biovision.com
- Shams, S. F. & Mehrad-Majd, H. TNFα-308G>a polymorphism and susceptibility to immune thrombocytopenia purpura (ITP): Evidence from a systematic review and meta-analysis. Cytokine 177, 156538. https://doi.org/10.1016/j.cyto.2024.156538 (2024).
- 77. Jang, D. et al. The role of tumor necrosis factor alpha (TNF-α) in autoimmune disease and current TNF-α inhibitors in therapeutics. *Int. J. Mol. Sci.* 22, 2719. https://doi.org/10.3390/ijms22052719 (2021).
- Alizadeh, A. A., Morris, M. B., Church, W. B., Yaqoubi, S. & Dastmalchi, S. A mechanistic perspective, clinical applications, and phage-display-assisted discovery of TNFα inhibitors. *Drug Discovery Today* 27, 503–518. https://doi.org/10.1016/j.drudis.2021.09 .024 (2022).
- 79. Zelova, H. & Hošek, J. TNF-a signalling and inflammation: interactions between old acquaintances. *Inflamm. Res.* 62, 641–651. https://doi.org/10.1007/s00011-013-0633-0 (2013).

- 80. Bradley, J. R. TNF-mediated inflammatory disease. J. Pathol. 214, 149-160. https://doi.org/10.1002/path.2287 (2008).
- 81. Zhang, H., Shi, N., Diao, Z., Chen, Y. & Zhang, Y. Therapeutic potential of TNFα inhibitors in chronic inflammatory disorders: Past and future. *Genes Diseases* 8, 38–47. https://doi.org/10.1016/j.gendis.2020.02.004 (2021).
- 82. Valesini, G. et al. Biological and clinical effects of anti-TNFα treatment. Autoimmun. Rev. 7, 35–41. https://doi.org/10.1016/j.autre v.2007.03.003 (2007).
- 83. Enzyme-linked Immunosorbent Assay Kit, for Tumor Necrosis Factor Alpha (TNFa), Cloud-Clone Corp., 23603 W, Fernhurst Dr., Unit 2201, Katy, TX 77494, USA.
- 84. Liu, M. et al. The histone methyltransferase EZH2 mediates tumor progression on the chick chorioallantoic membrane assay, a novel model of head and neck squamous cell carcinoma. *Transl. Oncol.* 6, 273–281. https://doi.org/10.1593/tlo.13175 (2013).
- 85. Busch, C., Krochmann, J. & Drews, U. The chick embryo as an experimental system for melanoma cell invasion. PLoS ONE 8, e53970. https://doi.org/10.1371/journal.pone.0053970 (2013).
- 86. Schmiech, M. et al. Comparative investigation of frankincense nutraceuticals: Correlation of boswellic and lupeolic acid contents with cytokine release inhibition and toxicity against triple-negative breast cancer cells. *Nutrients* 11, 2341. https://doi.org/10.3390/nu11102341 (2019).
- 87. Girgis, A. S., Tala, S. R., Oliferenko, P. V., Oliferenko, A. A. & Katritzky, A. R. Computer-assisted rational design, synthesis, and bioassay of nonsteroidal anti-inflammatory agents. *Eur. J. Med. Chem.* **50**, 1–8. https://doi.org/10.1016/j.ejmech.2011.11.034 (2012).
- 88. Tiwari, A. D. et al. Microwave assisted synthesis and QSAR study of novel NSAID acetaminophen conjugates with amino acid linkers. Org. Biomol. Chem. 12, 7238–7249. https://doi.org/10.1039/C4OB01281J (2014).
- 89. CODESSA-Pro manual, (accessed 29 June 2025); http://www.codessa-pro.com/manuals/manual.htm

Acknowledgements

This work was supported financially by National Research Centre, Egypt, project ID: 13060103.

Author contributions

A.S.G., M.S.B., and S.S.P. made conceptions; M.S.B., and A.S.G. made chemical synthesis; B.M.K. made X-ray studies; W.F, M.A.E, A.A.E.S., and S.M.H. made the antiproliferation and 3D-spheroid studies; A.A, S.N., and S.M.H. made the chicken embryo studies; A.S.G., and M.S.B. made the computational studies; B.M.K., S.S.P., M.S.B., and A.S.G. wrote the draft version; A.F. supervision; All authors have read and agreed to the published version of the manuscript.

Funding

Open access funding provided by The Science, Technology & Innovation Funding Authority (STDF) in cooperation with The Egyptian Knowledge Bank (EKB). No funding was received due to this study.

Declarations

Competing interests

The authors declare no competing interests.

Additional information

Supplementary Information The online version contains supplementary material available at https://doi.org/10.1038/s41598-025-20712-4.

Correspondence and requests for materials should be addressed to M.S.B. or A.S.G.

Reprints and permissions information is available at www.nature.com/reprints.

Publisher's note Springer Nature remains neutral with regard to jurisdictional claims in published maps and institutional affiliations.

Open Access This article is licensed under a Creative Commons Attribution 4.0 International License, which permits use, sharing, adaptation, distribution and reproduction in any medium or format, as long as you give appropriate credit to the original author(s) and the source, provide a link to the Creative Commons licence, and indicate if changes were made. The images or other third party material in this article are included in the article's Creative Commons licence, unless indicated otherwise in a credit line to the material. If material is not included in the article's Creative Commons licence and your intended use is not permitted by statutory regulation or exceeds the permitted use, you will need to obtain permission directly from the copyright holder. To view a copy of this licence, visit https://creativecommons.org/licenses/by/4.0/.

© The Author(s) 2025